Analyzing the Effect of Structural Changes on Ligaments Surrounding the Glenohumeral Joint on its Range of Motion to Improve the Biomechanical Understanding of Frozen Shoulder

Tom Driessen, 4840925, ME51035 ME-BMD MSc Thesis

Supervised by Dr. Ajay Seth, TU Delft, 2024-2025

August 14, 2025

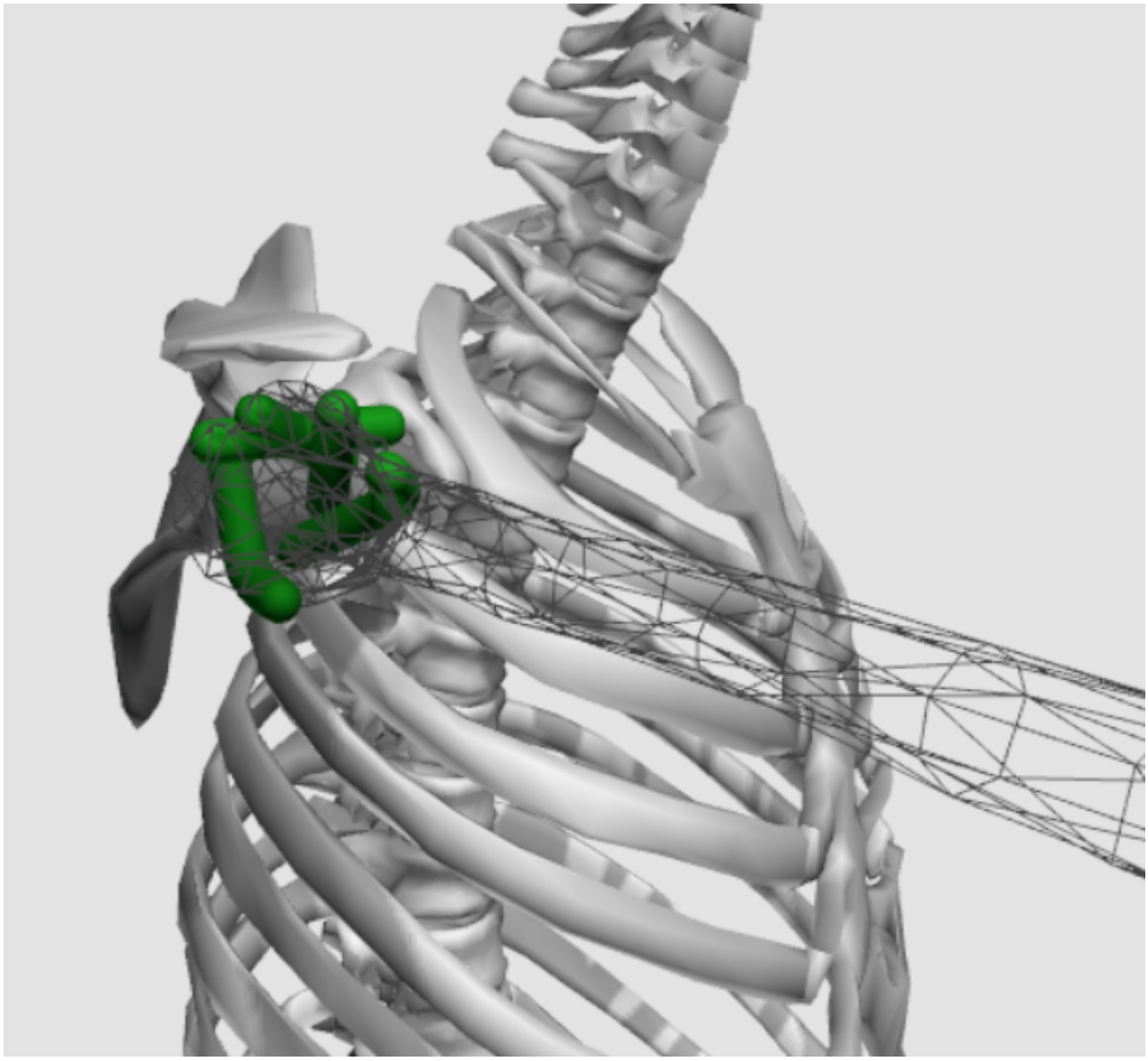

Contents

1 Introduction

1.1 Introduction to frozen shoulder

Frozen shoulder is characterized by four stages. In the pre-adhesive stage patients experience mild end-range pain. Patients in the freezing stage generally have a high level of discomfort as well as a high level of pain near the end-range of motion. In the frozen stage patients experience less pain but limited range of motion due to stiffness of the glenohumeral joint. The final phase is the thawing phase, characterized by stiffness without pain and regaining mobility of the arm [1]. Symptom duration can span over three years, with one study finding an average duration of 30 months [2, 3]. In over half the cases the range of motion remained restricted after the greatest recovery, though this rarely limited patients in their daily lives [3].

Frozen shoulder is a common injury with a prevalence of 2 to 5 % [4–9]. In patients with type II diabetes the prevalence is higher, ranging from 6 to 29% [4–8, 10]. Type II diabetes accounts for around 90% of the diabetes cases [11]. The upward trend in obesity is associated with a global increase in type II diabetes [11]. The current estimate of 536.6 million people between the age of 20 and 79 living with diabetes in 2021 is expected to increase by 46% to 783.2 million by 2045 [12]. This would cause the overall prevalence of frozen shoulder to increase as well.

In terms of healthcare costs, frozen shoulders costs the National Health Surface of the United Kingdom a minimum of £44.1 million or £110.3 million depending on the assumption of 2% or 5% prevalence [13]. One study found 84% of the patients to be between 40 and 59 years old [14]. Considering that these people are part of the working class and the duration of symptoms, frozen shoulder forms a substantial socioeconomic burden.

The etiology of frozen shoulder is poorly understood, where primary or idiopathic frozen shoulder has no known cause. Secondary frozen shoulder is generally attributed to trauma [1, 6, 15]. There are some conditions that increase the prevalence in these populations, like diabetes and thyroid disorders [16].

The directionality of the force exerted by the ligaments is determined by their points of attachment to the bones. This raises the question as to how the variation in attachment sites influences the range of motion of the glenohumeral joint. Research suggests that those with hypermobility in the shoulder joint may be less likely to develop frozen shoulder [17, 18]. Studying the range of motion determined by different attachment sites could provide insight into which configurations are at less risk, and perhaps even which configurations are at a higher risk of developing frozen shoulder.

1.2 Ligament attachment site variation

The glenohumeral ligaments play a prominent role in stabilizing the glenohumeral joint. Information about the attachment sites of the glenohumeral ligaments can be used by surgeons to recreate the anatomy prior to injury, which could restore the original kinematics [19, 20].

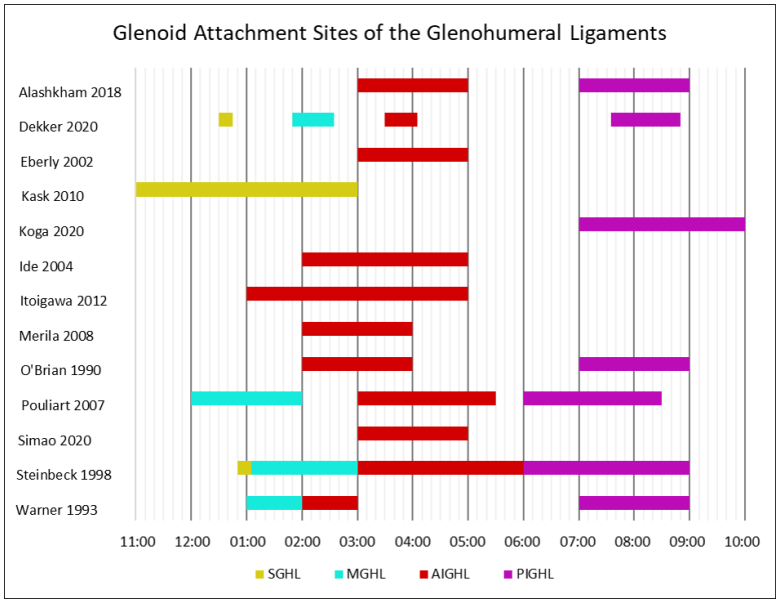

Figure 1: Visual representation of the range in attachment sites of the glenohumeral ligaments on the glenoid. SGHL: Superior Glenohumeral Ligament; MGHL: Medial Glenohumeral Ligament; AIGHL: Anterior Inferior Glenohumeral Ligament; PIGHL: Posterior Inferior Glenohumeral Ligament

A systematic review published in 2019 found 15 articles to either qualitatively or quantitatively report attachment sites of the glenohumeral ligaments. Quantitative data on glenoid attachment sites was provided by eight of those articles. No articles reported quantitative measurements on the humeral attachment sites [20]. An additional five articles have been identified and their results are summarized in table 1. For ease of comparison the results regarding the glenoid attachment sites have been visualized in fig. 1.

Most of the data on attachment sites comes from cadaver studies, only the study by Simao et al. used MRI data [32]. They found identical results to those reported by Alashkham and Eberly who investigated the same ligament on cadavers [26, 27].

For results to be more easily comparable and quantifiable, a clock face is projected on the glenoid or the humerus and ligament attachment sites are described by time ranges. As an example, O'Brian et al. found the AIGHL and PIGHL to attach to the glenoid between 2 and 4 o'clock and between 7 and 9 o'clock respectively. The projection of the clock face of the glenoid is described in three of the included articles [29,32,33]. The long axis of the glenoid serves as the 12 to 6 line, where the superior point is defined as 12 o'clock and the inferior point as the 6 o'clock position. The 3 o'clock position is on the anterior side of the glenoid at the midpoint of the long axis. The rest of the clock face can be determined from there. Dekker et al. adopted a slightly different method of finding the 12 o'clock position, using center of the origin of the biceps long head tendon. This tendon attaches at the supraglenoid tubercle which forms the highest point of the long axis of the glenoid [34]. Therefore the different methods of projecting the clock face should yield similar results.

The method of determining the clock face on the humeral head was described by Saito et al. [35]. This method was adopted by Dekker et al., which was the only article that was found to quantitatively define the attachment sites on the humerus [21].

Table 1: Overview of attachment sites

Author, Publication Date	**Number of Shoulders Analyzed**	**Glenoid Attachment Site**	**Humerus Attachment Site**
Superior Glenohumeral Ligament			
Dekker et al., 2020 [21]	10	12:30-12:45 (range 12:15-1:10)	12:55-1:40 (range 12:20-2:20)
Kask et al., 2010 [22]	27	11-3	-
Steinbeck et al., 1998 [23]	104	1	-
Medial Glenohumeral Ligament			
Dekker et al., 2020 [21]	10	1:50-2:35 (range 12:50-3:10)	2:10-3:35 (range 1:20-4:40)
Pouliart et al., 2007 [24]	100	12-2	-
Steinbeck et al., 1998 [23]	104	1-3	-
Warner et al., 1993 [25]	12	1-2	-
Anterior Inferior Glenohumeral Ligament			
Alashkham et al., 2018 [26]	140	3-5	-
Dekker et al., 2020 [21]	10	3:30-4:05 (range 2:35-5:00)	4:05-5:10 (range 3:10-5:45)
Eberly et al., 2002 [27]	10	3-5	-
Ide et al., 2004 [28]	84	2 (14.5%) 3 (64.5%) * 4 (14.5%) 5 (6.5%)	-
Itoigawa et al., 2012 [29]	60	1-3 (2%) 2-3 (60%) * 2-4 (18%) 3-4 (13%) 3-5 (5%) 4-5 (2%)	-
Merila et al., 2008 [30]	22	2-4	-
O'Brian et al., 1990 [31]	11	2-4	-
Pouliart et al., 2007 [24]	100	3-5:30	-
Simao et al., 2020 [32]	93 (MRI)	3 (15%) 4 (62.4%) * 5 (22.6%)	-
Steinbeck et al., 1998 [23]	104	2-9 **	-
Warner et al., 1993 [25]	12	1-3	-
Posterior Inferior Glenohumeral Ligament			
Alashkham et al. 2018 [26]	140	7-9	-
Dekker et al., 2020 [21]	10	7:35-8:50 (range 6:45-9:45)	7:20-8:50 (range 6:45-10:15)
Koga et al., 2020 [33]	50	7-8 (30%) 7:30-8:30 (22%) 8-9 (44%) * 9-10 (4%)	-
O'Brian et al., 1990 [31]	11	7-9	-
Pouliart et al., 2007 [24]	100	6-8:30	-
Steinbeck et al., 1998 [23]	104	2-9 **	-
Warner et al., 1993 [25]	12	7-9	-
Coracohumeral Ligament			
Dekker et al., 2020 [21]	10	-	11:55-12:40 (range 11:25-1:05)

*: For articles that reported on a range of attachment sites (Ide, Itiogawa, Koga and Simoa) a * is used to indicate the most prevalent attachment site.
**: Steinbeck et al. did not differentiate between the different bands of the inferior glenohumeral ligament, so the range indicated here resembles the combination of the anterior and posterior inferior glenohumeral ligament

1.3 Anatomical changes associated with frozen shoulder

Research has shown that there are changes in the joint capsule and ligaments that are associated with frozen shoulder. Histological findings include an increase of fibroblasts and contractile myofibroblast [36–39]. The anterior part of the capsule also shows fibrosis and increased presence of cytokines [36, 40].

Studies also show that there is shortening of the ligaments [41, 42], increased thickness [43–51] and increased stiffness [43–46, 52–54]. A systematic review on frozen shoulder suggests chronic inflammation, fibrosis and

glenohumeral joint capsule contracture to be responsible for the pain and limited range of motion [55]. As a result, most treatment options aim to lengthen the glenohumeral joint structures in an attempt to regain range of motion [56].

The results of eleven studies that looked into changes in stiffness and thickness of tissues surrounding the glenohumeral joint have been visualized in fig. 2 [43–51, 53, 54]

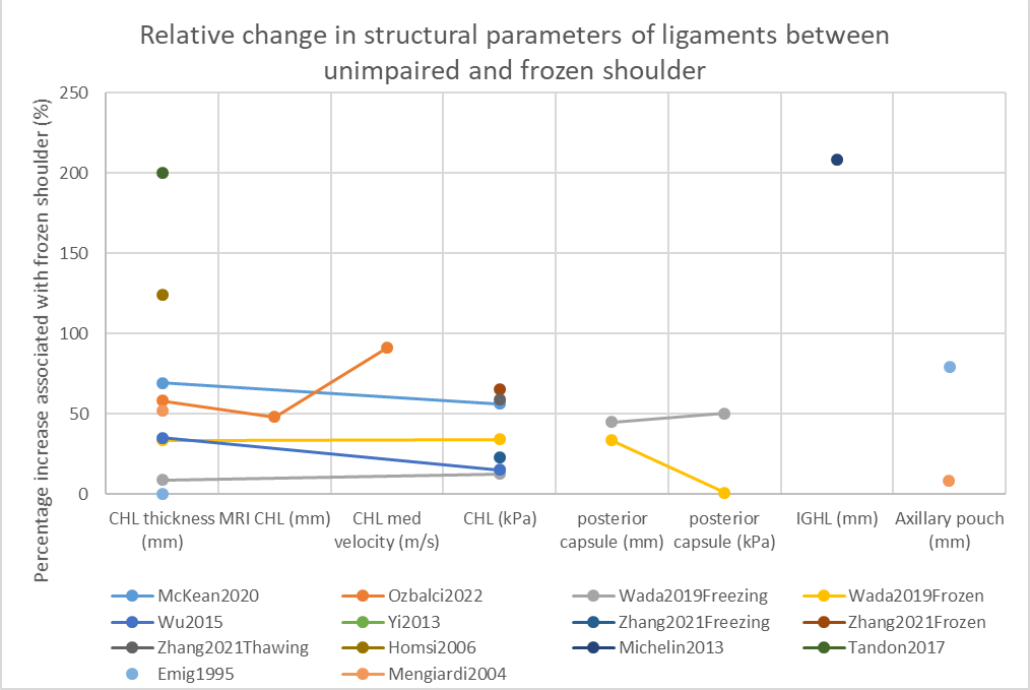

Figure 2: Percentual changes of different tissues surrounding the glenohumeral joint as seen in frozen shoulder. CHL: coracohumeral ligament; IGHL: inferior glenohumeral ligament

1.4 Problem definition

In order to better understand frozen shoulder, this study will focus on the impact of changes to ligament paths and their mechanical properties on the glenohumeral joint range of motion.

In their book on physical diagnostics, De Jongh et al. state that a passive limitation of the glenohumeral joint of over 50% during at least 3 months is indicative of frozen shoulder [57]. Similar criteria are used by Erber et al., where they require a loss of 50% of the internal rotation, 50% of the external rotation and 50% of the shoulder flexion or abduction [58, 59].

This study aims to answer the following research question: can the length or stiffness changes described in literature account for the 50% change in range of motion as seen in frozen shoulder?

Finding the answer to this question will help determine the relative importance of stretching and mobility exercises in frozen shoulder. Using the model, the strain of the ligaments can be determined for each pose across the full range of motion. This data can be converted to strain maps, which show the strain for all the combinations of two of the degrees of freedom. This makes it relatively easy to identify which poses result in high strain and should therefore be avoided, and which poses are safe. These strain maps of the different ligaments may indicate which ligaments are the cause of frozen shoulder and could then be used to determine which poses are effective at stretching the ligaments that limit the range of motion in frozen shoulder. Analyzing the effect the ligament stiffness has on the joint moment could be helpful for physiotherapist to determine which ligament or combination of ligaments is affected and the effect of attachment site variation.

2 Method

To investigate the effect of changes to the ligament paths, stiffness and length on the range of motion, OpenSim will be used [60]. The Thoracoscapular Shoulder Model [61] will be adapted to include ligaments spanning the glenohumeral joint.

2.1 Model adaptation

The glenohumeral joint is covered by muscles and tendons that allow the arm to move with respect to the scapula. The joint is encapsulated in the joint capsule. This capsule is reinforced by glenohumeral ligaments (GHLs) [62]. The four main components of the glenohumeral ligament complex are the superior glenohumeral ligament (SGHL), the medial GHL (MGHL) and the anterior inferior and posterior inferior GHLs (AIGHL and PIGHL respectively) [63]. The coracohumeral ligament (CHL) plays an important role in limiting the range of motion in frozen shoulder patients and was therefore also added to the model [64].

2.1.1 Determining the attachment sites based on literature

For the model to represent the biological situation it is important that the attachment sites of the ligaments are the same in the model as they are in the body.

From the articles that were used to quantify the attachment sites of the glenohumeral ligaments, it became clear that these attachment sites vary substantially from person to person. For instance, Ide et al. found the MGHL to have the same origin on the glenoid as the SGHL in 43.4% of the 84 cases they studied [28].

Since the article by Dekker et al. was the only article that quantified humeral attachments, and the attachments they found for the glenoid are in line with the results from the other papers, their results were used for generating the model.

In OpenSim, the attachment site of a ligament is given as a point. As the results gave a range over which the ligament attaches, the center of this range is used as the attachment site. For instance, the SGHL attaches between 12:30 and 12:45 on the glenoid and the attachment point for the model would be taken at 12:37.5. The mean attachments and the full range are summarized in table 2 for each ligament. The CHL attaches to the coracoid process instead of the glenoid. The attachment sites for the coracoid attachment varied by 1.4 mm around the mean attachment site along the long axis of the coracoid process.

Table 2: Overview of attachment site variation as found by Dekker et al. [21]

Ligament	Mean Attachment	Attachment Range
Glenoid		
Superior GlenoHumeral Ligament	12:30 - 12:45	12:15 - 1:10
Medial GlenoHumeral Ligament	1:50 - 2:35	12:50 - 3:10
Anterior Inferior GlenoHumeral Ligament	3:30 - 4:05	2:35 - 5:00
Posterior Inferior GlenoHumeral Ligament	7:35 - 8:50	6:45 - 9:45
Humerus		
CoracoHumeral Ligament	11:55 - 12:40	11:25 - 1:05
Superior GlenoHumeral Ligament	12:55 - 1:40	12:20 - 2:20
Medial GlenoHumeral Ligament	2:10 - 3:35	1:20 - 4:40
Anterior Inferior GlenoHumeral Ligament	4:05 - 5:10	3:10 - 5:45
Posterior Inferior GlenoHumeral Ligament	7:40 - 8:50	6:45 - 10:15

For each ligament the mean attachment sites were used, as well as the two endpoints of the attachment range. The size of the range of the mean attachments were used to determine the length over which the ligament attaches. The model requires point coordinates for the attachment site, so the center of these time ranges were used for these coordinates. To find the coordinates at the endpoints of the range, half of the attachment length was subtracted from or added to the endpoint. The timestamps of the different attachment points are shown in table 3. The attachments for the glenoid and humerus are also visualized in fig. 3 part A and B respectively.

Table 3: Overview of attachment site timestamps

Ligament	Lower Bound Attachment	Mean Attachment	Upper Bound Attachment
Glenoid			
Superior GlenoHumeral Ligament	12:225	12:375	1:025
Medial GlenoHumeral Ligament	1:125	2:125	2:475
Anterior Inferior GlenoHumeral Ligament	2:525	3:475	4:425
Posterior Inferior GlenoHumeral Ligament	7:225	8:125	9:075
Humerus			
CoracoHumeral Ligament	11:475	12:175	12:425
Superior GlenoHumeral Ligament	12:425	1:175	1:575
Medial GlenoHumeral Ligament	2:025	2:525	3:575
Anterior Inferior GlenoHumeral Ligament	3:425	4:375	5:125
Posterior Inferior GlenoHumeral Ligament	7:20	8:15	9:40

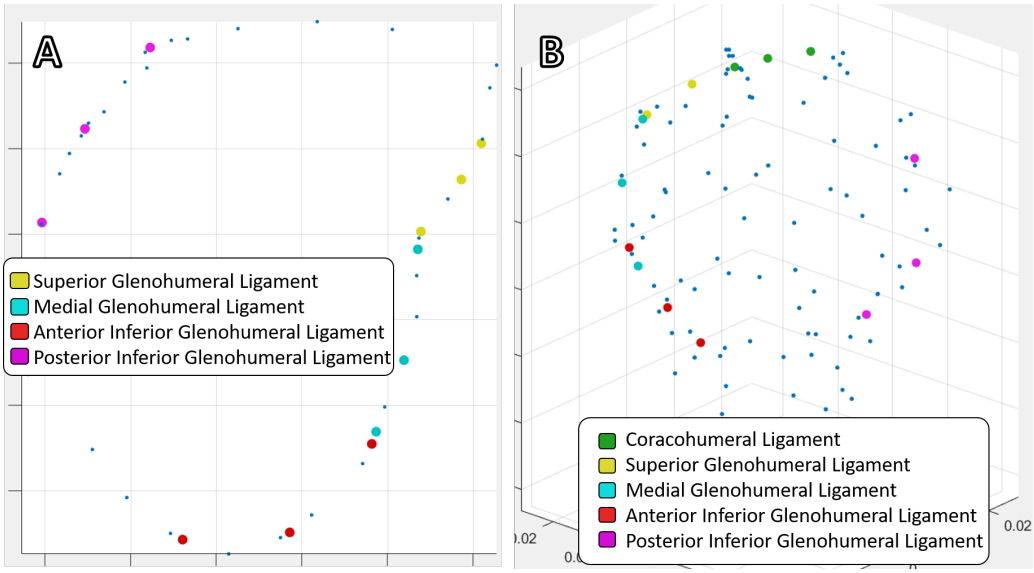

Figure 3: Image A shows the lower bound, mean and upper bound attachment sites for the SGHL, MGHL, AIGHL and PIGHL on the glenoid ring. The CHL attachment is not shown as this attaches to the coracoid process. Image B shows the lower bound, mean and upper bound attachment sites for all ligaments on the humeral head.

To get a better understanding of the impact of the attachment sites to the range of motion an additional 4 models were created: one where the ligaments attach to the lower bound on the scapula and the mean attachment on the humerus (called the -o configuration); one where the ligaments attach to the mean scapula attachment and lower bound on the humerus attachment (o- configuration), one where the ligament attaches from the mean attachment on the scapula to the upper bound of the humerus (o+ configuration) and finally a model where the ligaments attach to the upper bound on the scapula and the mean attachment on the humerus (+o configuration).The naming convention for the configurations uses -, o and + signs to indicate lower bound, mean and upper bound attachments in that order. The first sign indicates the scapular attachment and the second sign is used for the humeral attachment.

2.1.2 Finding the corresponding attachment sites of the glenoid

The method to match the attachment site locations from literature to the model is described below.

The first step was to obtain the mesh points from the 'scapula.vtp' and 'humerus.vtp' files in the 'Geometry' folder. These files are used to generate the scapula and humerus of the model.

The glenoid, the distal concave-shaped end of the scapula, forms the glenohumeral joint together with the humeral head. The mesh points of the glenoid were manually selected and depicted in red in fig. 4. There are a total of 31 points that make up the glenoid in this file. If these points are equally spaced around the glenoid that would give a resolution of 11.6°.

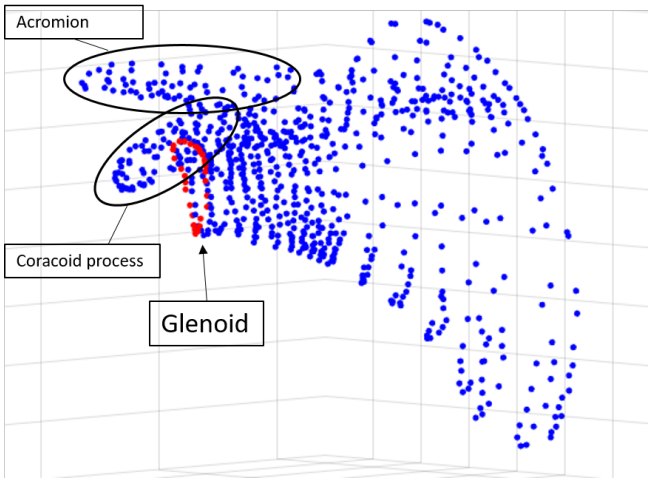

Figure 4: Scatter plot of the mesh points that make up the scapula. The points that represent the glenoid are shown in red. For clarification, the mesh points that comprise the coracoid process and acromion are circled.

The insertion points as found from literature were all located at time stamps that are multiples of 2.5 minutes (e.g. 1 hour and 17.5 minutes). Therefore the resolution needed to be brought down to 1.25° (12*24/360). Piecewise Cubic Hermite Interpolating Polynomial (pchip) was used to increase the number of mesh points by a factor of 1000. This method was preferred due to its ability to closely follow the original shape made by the 31 points.

The long axis of the glenoid determines the 12 o'clock location [29, 32, 33]. To find the long axis, the two points furthest apart were located. Of these two points, the one with the largest y-value was set as the 12 o'clock point. The angle from the center of the glenoid to this point to the horizontal was calculated. From this angle, 1.25° steps around the center of the glenoid were taken and used as reference. Similarly, the angle to the horizontal of the interpolated mesh points was calculated. These values were compared to the reference, where the closest value for each of the reference angles was stored.

The average absolute difference between the reference angles and the angles of the mesh points was found to be 0.0037° with the largest difference being 0.013°. The length of the long axis was found to be 0.035. Using this length and the largest error, the theoretical maximum error of the coordinate was found to be 8.1×10^{-6} m. Given that the X, Y and Z attachments in the GeometryPath property in the OpenSim GUI offer 3 decimal places, this was deemed accurate enough.

2.1.3 Finding the corresponding attachment sites of the humeral head

Whereas the ligaments on the glenoid attach to the glenoid rim, the attachment on the humerus is less easily determined. An article by Momma et al. analyzed the thickness variation of the shoulder joint capsule [65]. They included a figure of the area at which the joint capsule attaches to the humerus, see fig. 5.

Similarly to finding the attachment sites on the scapula, the mesh points were loaded into Matlab. Using a combination of the existing mesh points and points between the existing mesh points, a ring was created around the humeral head. The goal was for this ring to closely follow the white dashed line in fig. 5 closest to the joint surface. Again, pchip was used to interpolate the points by a factor 1000. This ring is visualized in fig. 6. For the lateral view, the S shape as seen in fig. 5 C was tried to replicate.

The point with the smallest y value was taken as the 6 o'clock position and in a similar fashion as for the glenoid, 1.25° steps around the center of the ring were taken and used as reference. Similarly, the angle to the horizontal of the interpolated mesh points was calculated. These values were compared to the reference, where the closest value for each of the reference angles was stored.

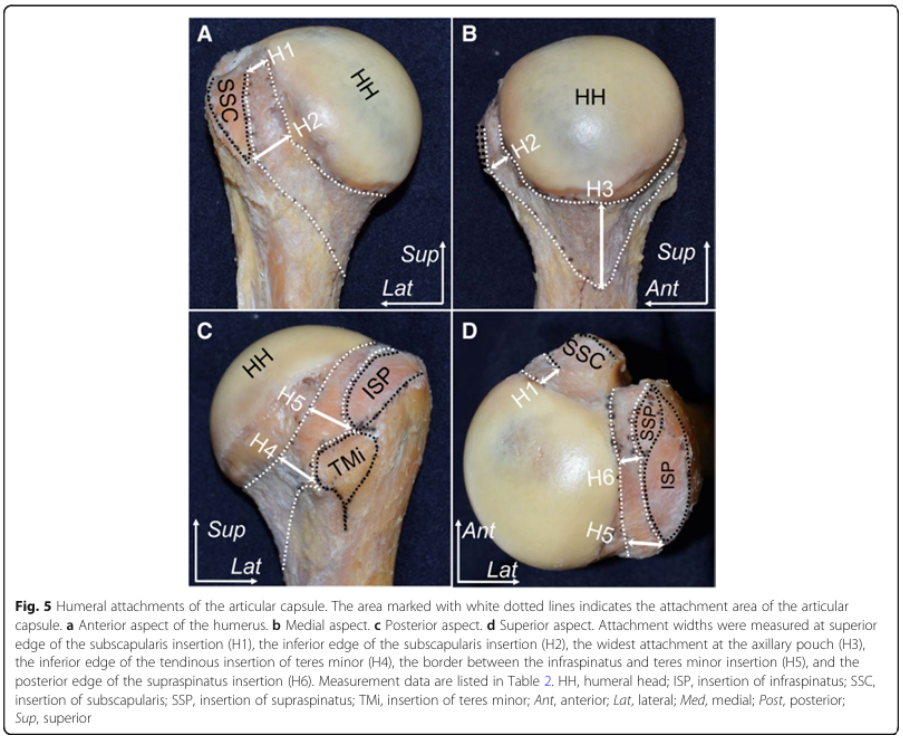

Fig. 5 Humeral attachments of the articular capsule. The area marked with white dotted lines indicates the attachment area of the articular capsule. **a** Anterior aspect of the humerus. **b** Medial aspect. **c** Posterior aspect. **d** Superior aspect. Attachment widths were measured at superior edge of the subscapularis insertion (H1), the inferior edge of the subscapularis insertion (H2), the widest attachment at the axillary pouch (H3), the inferior edge of the tendinous insertion of teres minor (H4), the border between the infraspinatus and teres minor insertion (H5), and the posterior edge of the supraspinatus insertion (H6). Measurement data are listed in Table 2. HH, humeral head; ISP, insertion of infraspinatus; SSC, insertion of subscapularis; SSP, insertion of supraspinatus; TMi, insertion of teres minor; *Ant*, anterior; *Lat*, lateral; *Med*, medial; *Post*, posterior; *Sup*, superior

Figure 5: Image taken from the paper by Momma et al. showing the attachment area of the shoulder joint capsule [65]

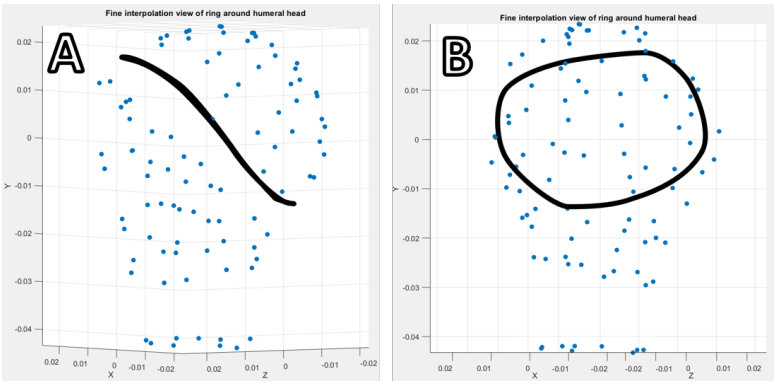

Figure 6: Ring around the humeral head on which the ligaments attach. Figure A: lateral view. Figure B: frontal view

Ligaments of the Blankevoort1991Ligament class were added to the model. The coordinates found through the method described above were used for the attachment coordinates to the humerus and scapula. The configuration of these ligaments implemented in the model can be found in fig. 7.

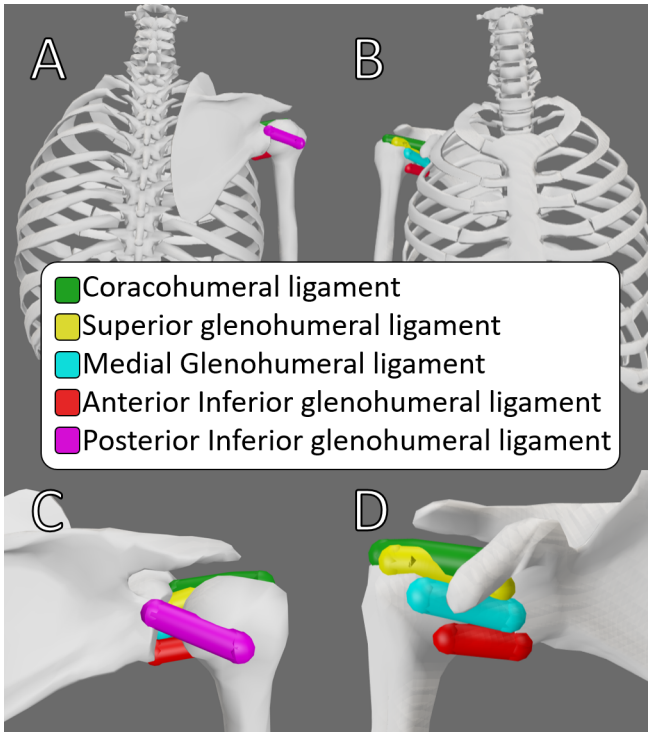

Figure 7: Image of the OpenSim model showing the added ligaments. A: posterior view; B: anterior view; C: Posterior view, zoomed in; D: anterior view, zoomed in, without thorax

2.1.4 Finding the rest lengths of the ligaments

The ligaments around the glenohumeral joint prevent the joint from reaching extreme angles [66]. In order to set the rest lengths so the ligaments engage at the extremes of the range of motion, the healthy range of motion needs to be known. Unfortunately, there is limited quantitative data on the healthy range of motion for the glenohumeral joint.

When lifting the arm upwards, for instance until the arm is horizontal, the humerus is at an angle of 90° with respect to the thorax. This angle is known as the humerothoracic angle. Data on the humerothoracic range of motion is more extensive but this does not directly relate to the glenohumeral angle, which is the angle between the humerus and the scapula. During movement of the arm, the humerus moves with respect to the scapula, which in turn moves with respect to the thorax. These movements are separated in the scapulohumeral rhythm. This is a ratio that determines how much of the humerothoracic angle is due to glenohumeral angle and the scapulothoracic angle [67].

The scapulohumeral rhythm is dependent on the plane of elevation. Different studies have looked into this

and found the scapulohumeral rhythm for the abduction plane to be 2.1 (2.0-2.3), for the scaption plane to be 1.9 (1.6-2.1) and for forward flexion to be 1.7 (1.1-2.0) [67–70].

Studies that analyzed the glenohumeral range of motion reported values for maximum shoulder elevation as 86° and 90° [71, 72].

Apart from the glenohumeral shoulder elevation, there are two more degrees of freedom in the glenohumeral joint. The plane of elevation determines the direction in which the arm points when it is lifted. For instance, when the plane of elevation is 0°, the arm points towards the side, parallel to the thorax. When the plane of elevation is 90°, the arm points straight ahead, perpendicular to the thorax. The last degree of freedom is the axial rotation, which is divided in internal and external rotation. When the humerus is elevated so that it is horizontal and the elbow is flexed 90°, moving the hand downward means internally rotating the glenohumeral joint. Moving the hand upwards corresponds to externally rotating the glenohumeral joint. These degrees of freedom of further clarified in fig. 8.

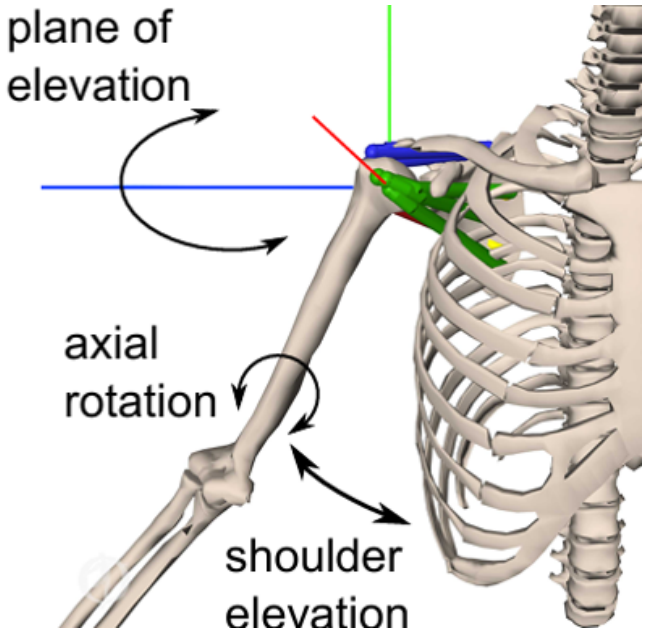

Figure 8: This figures shows the 3 degrees of freedom of the glenohumeral joint: shoulder elevation, plane of elevation and axial rotation. This image was taken from the work of Prendergast et al. [73]

Similarly to the shoulder elevation, there is limited data on the achievable plane of elevation and axial rotation for the glenohumeral joint specifically.

Several studies were found to report the maximum internal and external rotation for different combinations of shoulder elevation and plane of elevation [67, 71, 72, 74, 75]. To find the rest lengths of the ligaments, manual optimization was performed to match the results to this data and empirical tests carried out by the author. The viable range of motion for the glenohumeral joint was found to be -30° to 130° of planer elevation, -44° to 120° of shoulder elevation and -90° to 90° of axial rotation.

The rest lengths of the ligaments were found to be 0.05511 m for the coracohumeral ligament, 0.05376 for the superior glenohumeral ligament, 0.04294 for the medial glenohumeral ligament, 0.041258 for the anterior inferior glenohumeral ligament and 0.06315 for the posterior inferior glenohumeral ligament.

The rest length of the ligaments needed to be changed for the different configuration. To achieve this they were scaled by $\frac{L_{config}}{L_{mean}}$ where L_{mean} is the mean length of the ligament over the whole range of motion for the ligament with the mean attachment sites (oo). L_{config} is the mean length of the ligament over the whole range of motion for that specific configuration of the ligament.

A probability distribution of the lengths for the different ligaments are shown in fig. 9. The different configurations use the following naming convention: the first symbol (-, o, +) indicates the attachment on the scapula and the second symbol indicates the attachment the humerus. The - sign indicates the ligament is attached to the lower bound, the o that it is attached to the mean attachment site and the + that it is attached to the upper bound. As an example, -o represents the ligament that is attached to the lower bound on the scapula and the mean attachment site on the humerus. The oo configurations, shown in black, is considered to be the base model, with both the scapula and humerus attachments on the mean attachment site. L_{mean} is based on this model.

Each graph shows the distributions of the five different configurations for that ligament. Vertical lines of the same color indicate the rest length for that configuration. The values of these rest lengths are shown in fig. 9 F.

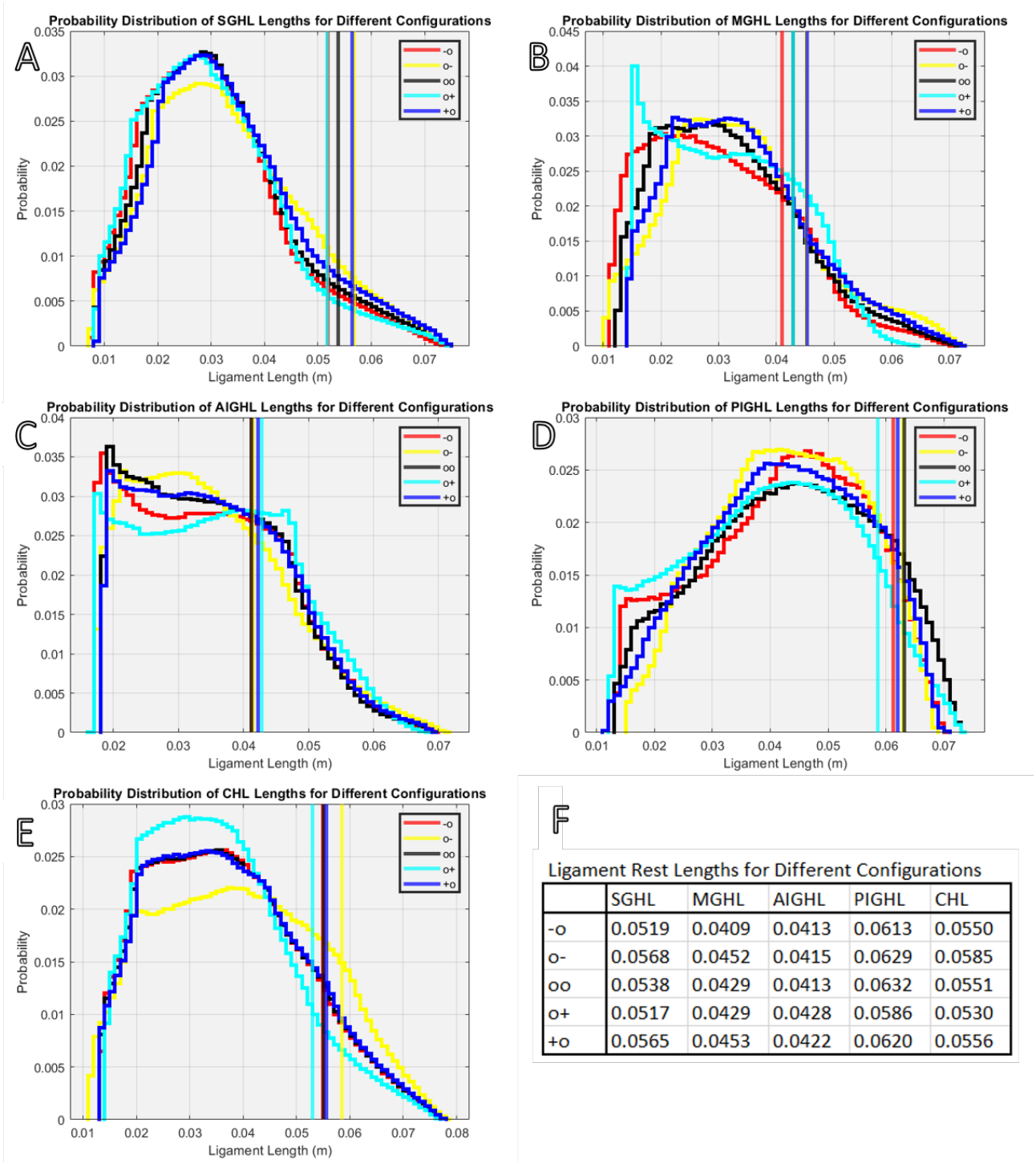

F

Ligament Rest Lengths for Different Configurations

	SGHL	MGHL	AIGHL	PIGHL	CHL
-o	0.0519	0.0409	0.0413	0.0613	0.0550
o-	0.0568	0.0452	0.0415	0.0629	0.0585
oo	0.0538	0.0429	0.0413	0.0632	0.0551
o+	0.0517	0.0429	0.0428	0.0586	0.0530
+o	0.0565	0.0453	0.0422	0.0620	0.0556

Figure 9: Probability distributions of the ligament lengths. Each of the graphs shows the distribution for one of the ligaments. Different colors indicate the distributions for different configurations. Vertical lines indicate the rest length for that configuration. A: distribution for the SGHL lengths; B: distribution for the MGHL lengths; C: distribution for the AIGHL lengths; D: distribution for the PIGHL lengths; E: distribution of the CHL lenghts; F: table showing the ligament rest lengths for each of the ligaments and configurations.

2.2 Changes associated with frozen shoulder

Several studies investigated changes in stiffness and thickness of tissues surrounding the glenohumeral joint. The result of these studies are visualized in fig. 2 [43–51, 53, 54].

There is a substantial spread in findings, with thickness changes of the coracohumeral ligament varying from 0% to 200% [49, 50]. Most studies reported on the thickness changes of structures around the joint and four studies reported both thickness and stiffness changes, or a derivation thereof [43–46]. From these studies there is roughly a 1 to 1 correlation between thickness change and stiffness change (1:0.92). On average there is a 66%

increase in thickness of these surrounding tissues and a 41% increase in stiffness. Only one study was found on the inferior glenohumeral ligament thickness change, which they reported to be 208%, the highest value among the included studies [48].

Given the large spread in reported values, as well as the fact that not all ligaments were reported on, a 50% stiffness increase will be assumed for all ligaments for analyzing the effects of frozen shoulder.

Despite the contracture of the joint capsule being mentioned in several studies, as well as the lengthening of these structures being the aim of most treatment options, no articles were found to quantitatively report on these length changes. To obtain information about length changes, the following formula was used:

$$k = E * \frac{A}{l}$$

where k is the stiffness, E is the Young's Modulus, A is the cross sectional area of the ligament and l is the length. Using the assumption that the volume of the ligament remains constant, i.e. $A_1 * l_1 = A_2 * l_2$, and assuming that the Young's Modulus does not change, the following formula can be obtained:

$$l_2 = \sqrt{\frac{k_1 * l_1^2}{k_2}}$$

where l_1 and l_2 the ligament lengths and k_1 and k_2 are the ligament stiffness in the healthy and frozen shoulder ligaments respectively.

Applying this to the earlier established 50% stiffness increase, a shortening of 18% is found. Using the data from McKean at el. the ligament length in frozen shoulder would be 20% less than in the healthy shoulder [43]. For the results, this will be used as the lower bound for all ligaments.

2.3 Effect of parameter changes on ligament force

Changing the attachments sites changes the wrapping of the ligament. Since the distance between the attachment sites is not constant this will also influence the ligament length over the range of motion.

Shortening of the ligaments, as is associated with frozen shoulder, is implemented in the model by lowering the ligament rest length. This is the length at which the ligament transitions from being slack to being under strain. The effect this has on the force exerted by the ligament is visualized in fig. 10. This figure shows three force-length curves. The blue line shows the baseline ligament, with a rest length of 1 cm. The yellow line shows the force-length curve for the same ligament, with the same stiffness but a rest length of 0.9 cm.

Due to the shorter rest length the ligament will be engaged at lengths were it used to slack. Additionally, the force exerted by the shorter ligament will exceed that of the baseline ligament at equal lengths. For example, when the ligament is stretched to a length of 1.1 cm, the baseline ligament will be under 10% strain, whereas the shorter ligament will be under 22.2% strain. This relative difference in strain increases if the rest length is decreased.

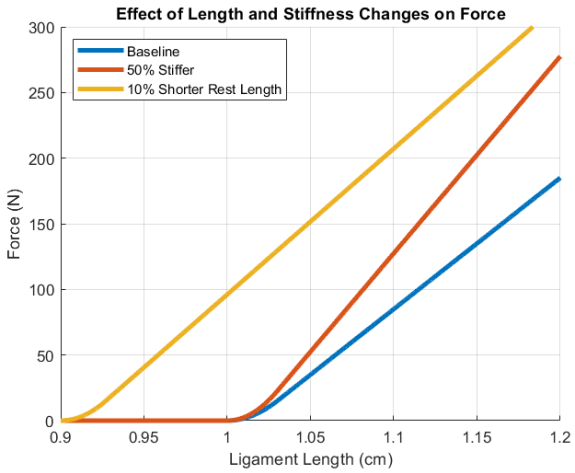

Figure 10: Force-length curve for a normal ligament with a rest length of 1 cm, a model with 50% stiffer ligament and a model with 10% shorter rest length.

Another change in structure that is associated with frozen shoulder is an increase in ligament stiffness. The orange line in fig. 10 shows the force-length curve of a ligament with 50% more stiffness than the baseline ligament. This translate to a 50% higher force for both the toe region and linear region.

2.4 Obtaining model data

In order to analyze the impact of length and stiffness changes on the ligament strain and joint moments three types of output were required from the model: ligament length, moment arms and force.

To obtain the ligament length, three for-loops were used to cover the determined range of the three degrees of freedom. This was done at a 2° resolution for each of the degrees of freedom, resulting in a 81x83x91 array for each of the ligaments. For all of the 611 793 poses the getLength functionality of the Blankevoort1991Ligament class was used to find the ligament length for that specific pose. This process took roughly one hour to complete on my machine and had to be repeated for the other models as the different configurations would result in different lengths.

Obtaining the moment arms for the three degrees of freedom was done in a similar method using the computeMomentArm functionality at comparable computational cost.

To obtain the force data, the OutputReporter was used. Unfortunately, due to the complexity of the model, this process was computationally much more expensive. Getting the ligament forces at 10° resolution took around one hour. To obtain these results at the same resolution as the length data, an estimated 125 hours would have been required (5^3, five times higher resolution for three degrees of freedom). To combat this, a simple model was created in OpenSim Creator [76]. It consisted of a single slider joint spanned by a ligament. Using increments of 0.01% strain the force exerted by this ligament was collected using the OutputReporter. This data was used to create a normalized force-length curve using a second order polynomial for the toe-region (between 0 and 3% strain) and a first order polynomial for the linear region (above 3% strain). This normalized force-length curve could than be scaled to match the desired ligament stiffness as taken from the model. Using the ligament lengths that were already obtained ligament force could be calculated for the full range of motion.

The results of this method were compared to results obtained directly from the OutputReporter at 10° resolution. On average a difference of 1.7×10^{-6}% was found. Using the largest difference of 5.87×10^{-5} Newton and given that the largest moment arm does not exceed 0.025 m, the maximum difference between these methods could be 1.5×10^{-6} Nm which was found to be acceptable.

Using this method it was possible to analyze the effect of combinations of length, stiffness and configuration changes. Generating the results for 42 combinations (7 different amounts of shortening and 6 different amounts of stiffness increase) for all five of the configurations would have taken close to three years. Using the described method it can be done in around three minutes.

2.5 Determining impact of length changes

To determine the impact of length changes, custom code was written in Matlab to determine the ligament lengths across the full range of motion. This was determined at a 2° resolution for each of the degrees of freedom, resulting in a 81x83x91 array for each of the ligaments. This data, combined with the rest lengths, could be used to determine the strain maps for each ligament. The impact of length changes was determined by multiplying the rest length by a factor smaller than 1, i.e. 0.8 in case of a 20% reduction in length. With this new rest length, the change in strain maps could be analyzed.

To further analyze the impact of these length changes, additional code was written to determine the minimum and maximum shoulder elevation and axial rotation at 5% strain. This border of 5% strain was based on the work of Ticker et al., who found the inferior glenohumeral ligament could fail at strains of around 9% in the middle of the ligament [77]. Continuing on this work Pollock et al. found that cyclic loading of as low as 4.6% strain could cause lasting elongation of the ligament in cadaver studies [78]. Although the source of pain is often poorly understood, straining the ligament results in muscle activation around that joint to protect and stabilize it [79]. Based on this information, the author assumes 5% strain to be around the limit of comfort.

This information was used to determine the percentage of shoulder elevation or axial rotation that was lost for each plane of elevation.

Lastly, the areas of the strain maps for the different planes of elevation within the 5% strain margin were compared to provide insight in the overall loss of range of motion associated with these length changes.

2.6 Determining impact of stiffness changes

Custom code was written in Matlab for the analysis of stiffness changes. The model was placed in different poses, covering the whole range of motion at 2° resolution. The forces in the ligaments and their moment arms were computed with normal stiffness and a 50% increase in stiffness to simulate the stiffness in frozen shoulder.

Once the forces and moment arms were calculated, they were multiplied and added together to find the contribution of the ligament forces on the joint torque. These values can be compared to the joint torque for the frozen shoulder case. This simulates the situation at the physiotherapist where the arm of the patient is passively moved around.

To quantify the effect of stiffness change on the range of motion, the ROM within a certain bound is taken. This boundary is determined by the joint moment. The force-strain curves of the different ligaments is visualized in fig. 11. The ligaments wrap over customized wrapping surfaces. This prevents the ligaments from going through the humeral head and ensures they follow a natural path across the range of motion. These wrapping surfaces have radii around 0.02 m, which gives an indication of the magnitude of the moment arm when the ligament is under strain. To get a better understanding of the effect of ligament stiffness changes on the joint moment, the moment that serves as a boundary needs to be carefully selected.

If the boundary is too small, for instance 0.1 Nm, it can be reached while the ligament is in the toe-region of the force-strain curve. Given the quadratic nature of this region, it is less sensitive to an increase in stiffness. If the boundary is set too high, for instance at 5 Nm, this will only be reached when the ligament produces 250 N of tensile force, assuming the moment arm to be 0.02 m. Depending on the ligament, this would occur between around 14% and 31% strain. When the strain values are that high it is likely the ligaments are damaged, making for an unsuitable boundary.

A boundary of 1 Nm seems to be able to provide insight on the effect of stiffness changes on the range of motion. Assuming the moment arm to be 0.02 m this would occur when the ligament exerts 50 Newtons of force. Depending on the ligament this occurs between 4.0 and 6.9% strain. Increasing the stiffness by 50% would result in the same force between 3.2 and 5.1% strain.

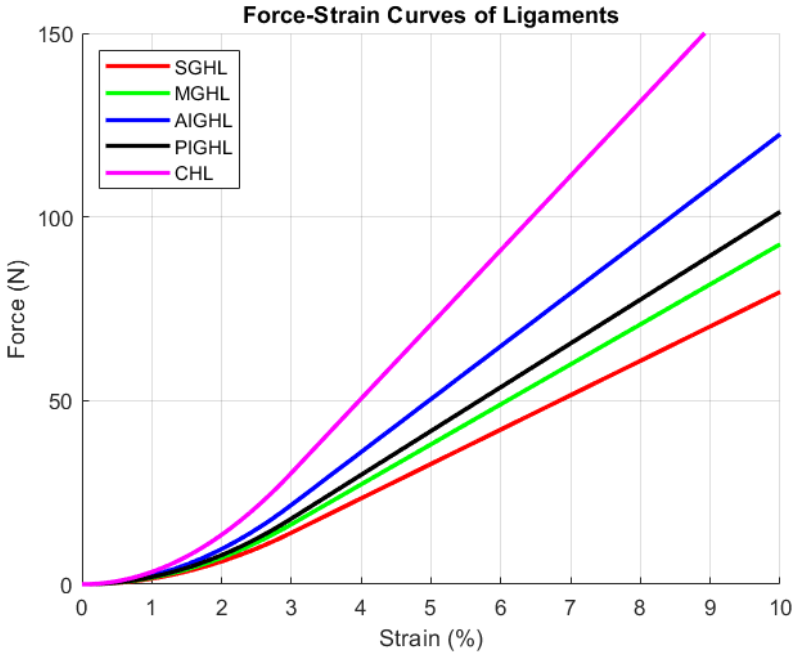

Figure 11: Force-strain curves of the coracohumeral and glenohumeral ligaments. The force-strain curves shown are based on the normal model, without increased stiffness.

3 Results

We present the effect of attachment site variation, length changes and stiffness changes on model passive range of motion and moments.

3.1 Impact of attachment site variation on range of motion

The impact of the variation in attachment sites of the SGHL, MGHL, AIGHL, PIGHL and CHL on the range of motion is visualized in fig. 12, fig. 13, fig. 14, fig. 15 and fig. 16 respectively.

These figures consist of five parts. Part A shows the shaded strain map, where the colored lines indicate the 5% strain borders for the different configurations. The part of the ROM that is within this border is shown in white. The area outside the border is shaded. The darkness of the shaded region is determined by the amount of configurations for which that area is outside of the border. If an area of the graph is shaded black, this means it is outside of the border for all of the configurations. Parts B, C and D show similar graphs that indicate what part of the ROM is within and outside of the border of 1 Nm for the different configurations. These graphs show the impact on the Axial Rotation moment, the Plane of Elevation moment and the Shoulder Elevation moment respectively. The horizontal axes of these graphs show the axial rotation, ranging from -90° to 90°. Negative

axial rotation indicates external rotation and positive axial rotation means internal rotation. The vertical axes represent shoulder elevation. The plane of elevation is set at 40°, which was determined to be the scaption plane. Lastly, part E is a row of images showing the orientation of the ligament in the model. The color of the border around these images is consistent with the colors used in the graphs.

The red line, -o therefore resembles the border of the ligament that attaches to the lower bound on the scapula and the mean attachment on the humerus. The yellow line, o- shows the ligament attached at the mean position on the scapula and the lower bound on the humerus. The black line, oo, shows the strain border for the ligament that attaches to the mean scapula and humerus position. The cyan line, o+, resembles the border of the ligament that is attached to the mean attachment on the scapula and the upper bound on the humerus. Finally, the blue line, +o, indicates the border of the ligament attached to the upper bound on the scapula and the mean attachment on the humerus.

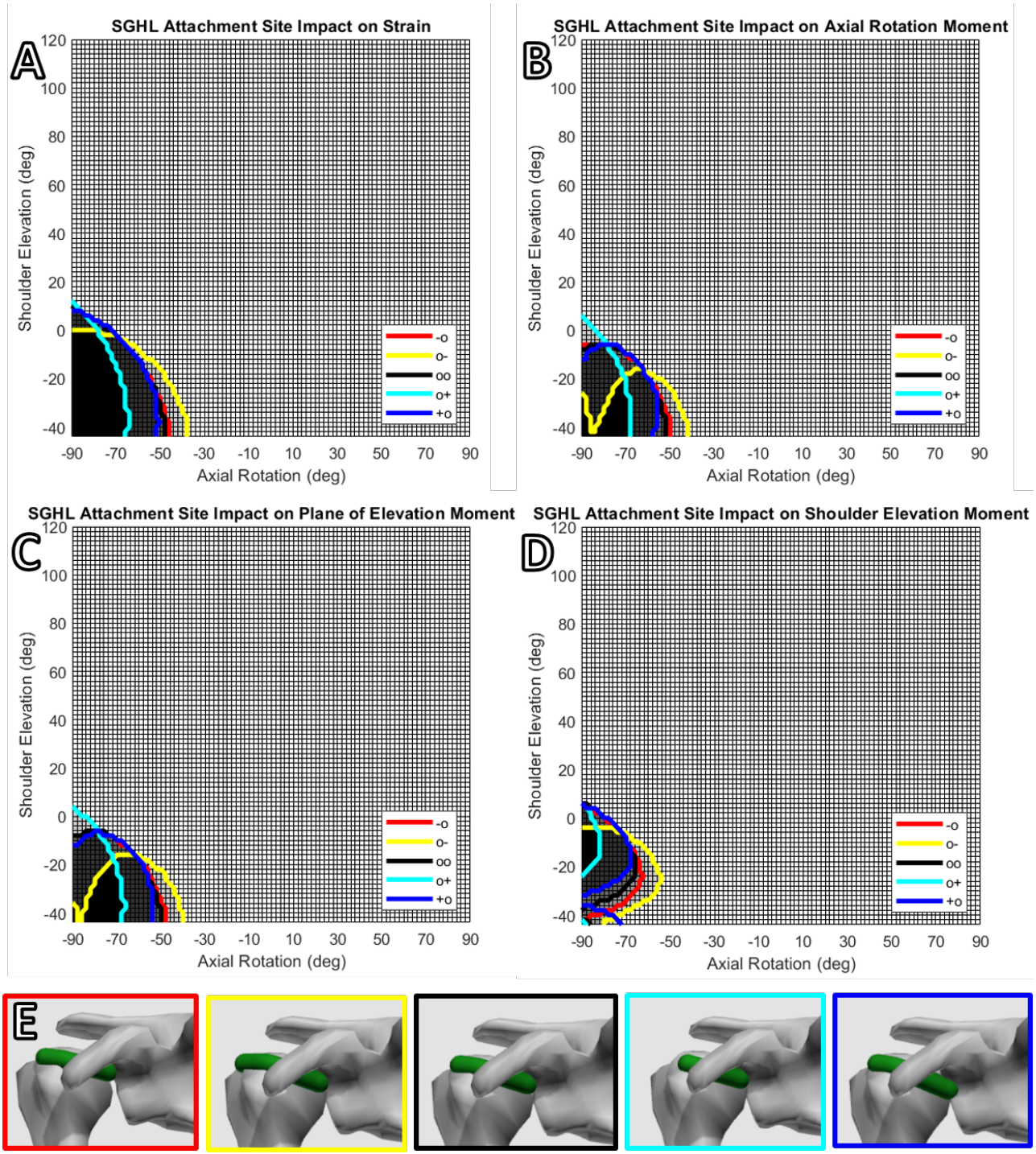

Figure 12: Impact of SGHL attachment site variation on the range of motion. A shows the strain map, using 5% strain as the border. B, C and D show moment maps for axial rotation, plane of elevation and shoulder elevation respectively, using 1 Nm as border. E shows the different configurations in the model

Looking at fig. 12 the SGHL limits extension and external rotation. It appears the attachment site on the scapula does not influence the strain map much. On the other hand, the attachment on the humerus seems to either increase or decrease the external rotation. This also translates to the graphs that show the moment (henceforth called moment maps). The red and blue lines stay close to the black line whereas the yellow and cyan lines deviate from it more.

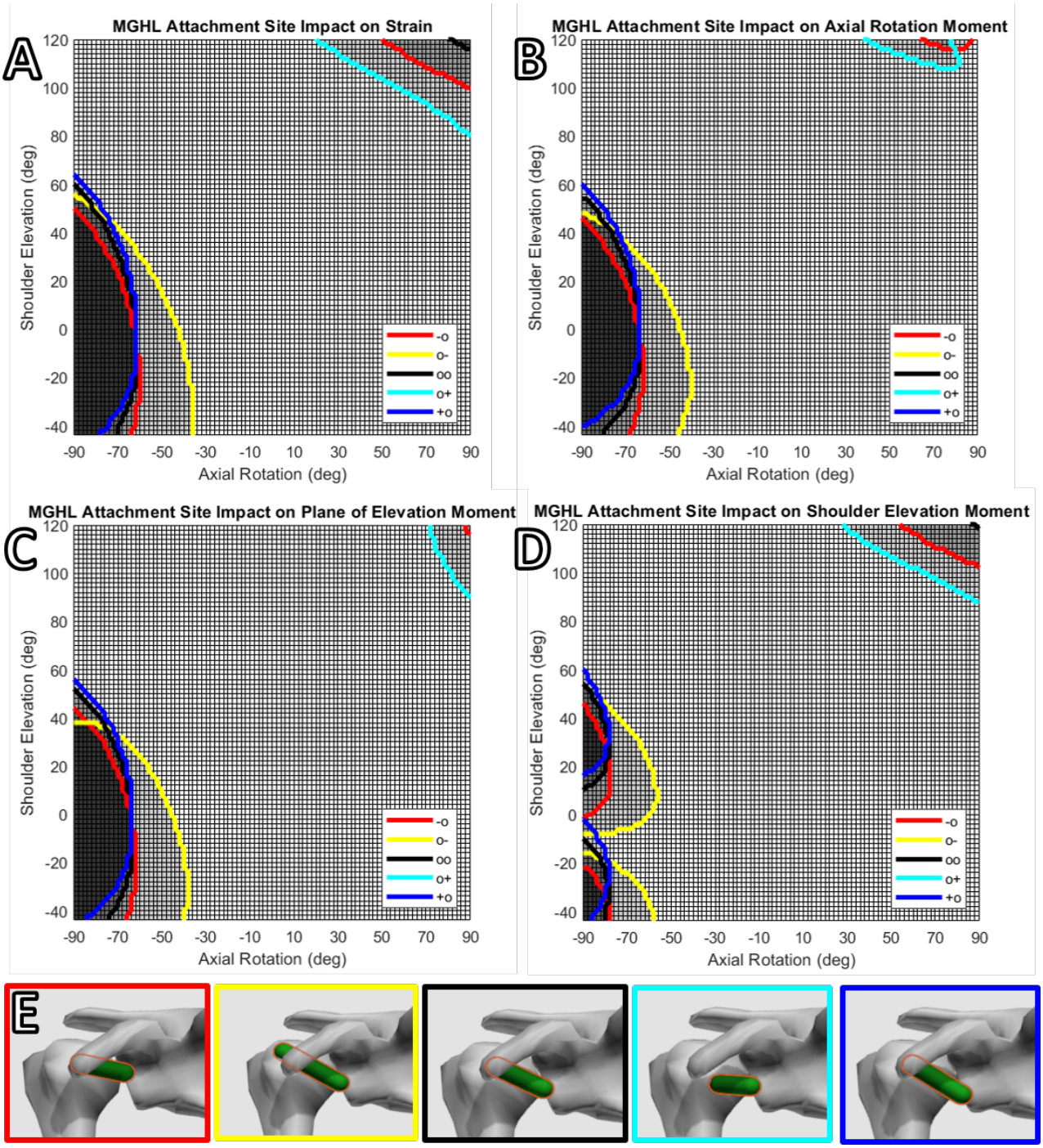

Figure 13: Impact of MGHL attachment site variation on the range of motion. A shows the strain map, using 5% strain as the border. B, C and D show moment maps for axial rotation, plane of elevation and shoulder elevation respectively, using 1 Nm as border. E shows the different configurations in the model

The MGHL, as shown in fig. 13, limits external rotation as well as internal rotation at high angles of shoulder elevation. Attaching to the upper bound on the humerus (o+) takes away the limit on external rotation. In return this configuration appear to limit the internal rotation more. Attaching to the lower bound on the humerus further limits the external rotation. Similar to the SGHL attachment site variation on the scapula has smaller impacts on the range of motion than changing the humeral attachment site. Due to the position of ligament, its moment arm for shoulder elevation is small for most configurations. This explains why there is

limited shaded area in fig. 13 D. In the bottom left corner of fig. 13 D the shaded areas are divided in two. This is due to the transition from a negative moment to a positive moment. In between these regions the moment arm drops to zero, causing the moment to remain below the threshold of 1 Nm.

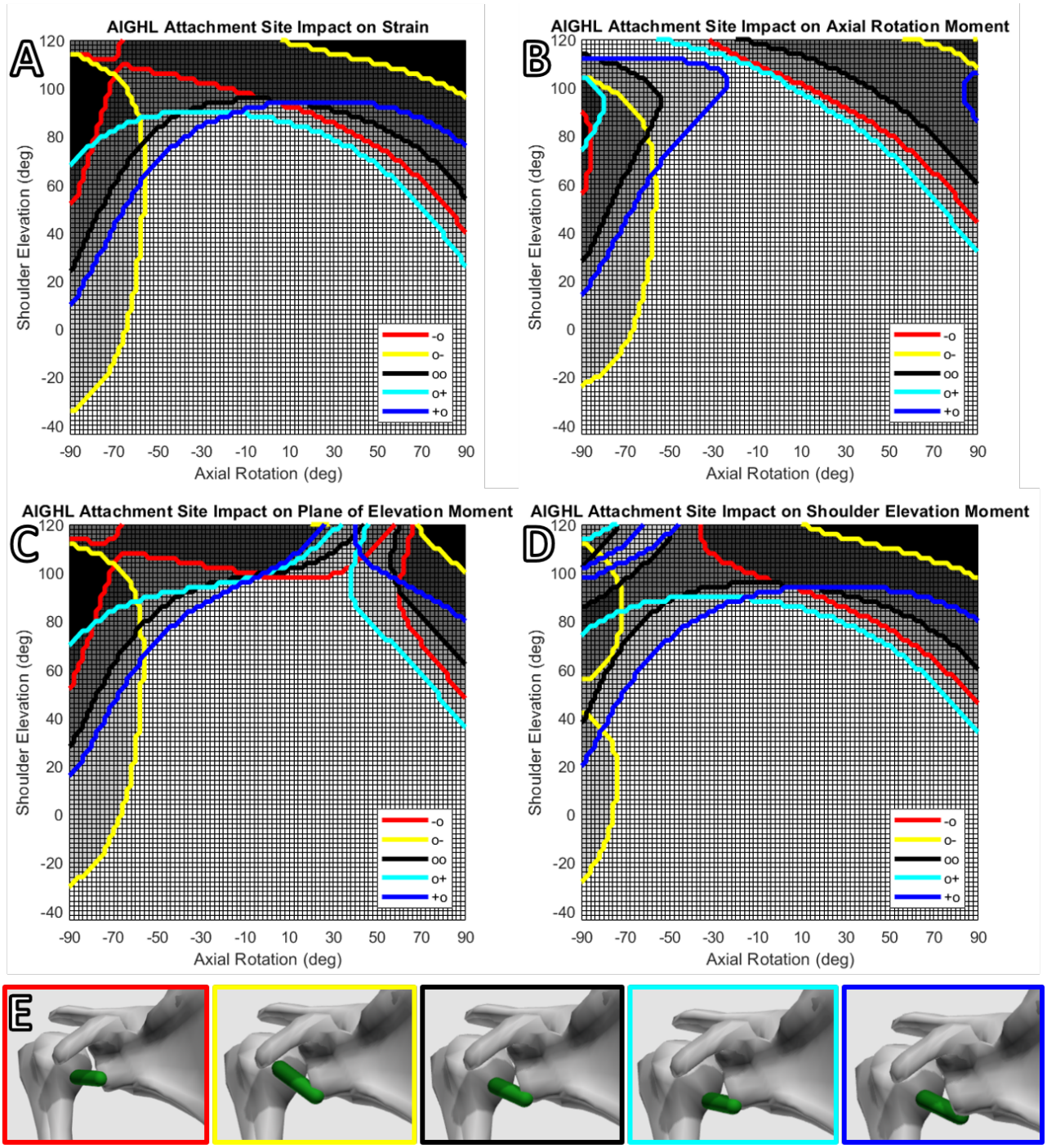

Figure 14: Impact of AIGHL attachment site variation on the range of motion. A shows the strain map, using 5% strain as the border. B, C and D show moment maps for axial rotation, plane of elevation and shoulder elevation respectively, using 1 Nm as border. E shows the different configurations in the model

For the mean attachment combination (oo) the AIGHL appears to limit glenohumeral elevation above 90°, while also limiting the external and internal rotation when the arm is elevated, as shown in fig. 14 A. Comparing the boundaries it seems that the attachment site on the scapula mainly determines the axial rotation, where the lower bound attachment (-o) allows for more external rotation with less internal rotation and the upper bound (+o) allows for more internal rotation while limiting the external rotation. The attachment on the humerus appears to have the opposite effect, where attachment to the lower bound (o-) limits the external rotation while allowing for more internal rotation. Additionally, the lower bound humeral attachment limits external rotation over a larger part of the shoulder elevation, while allowing for more shoulder elevation in general. This finding

holds when looking at fig. 14 D where the shoulder elevation moment of o- hardly exceeds the threshold. At small angles of axial rotation the AIGHL crosses between the humeral head and the scapula. These poses produce low strain, if any, while having a small moment arm. As a result, the axial rotation moment only exceeds the threshold at higher angles of axial rotation or shoulder elevation, where the ligament has to wrap around the humeral head more.

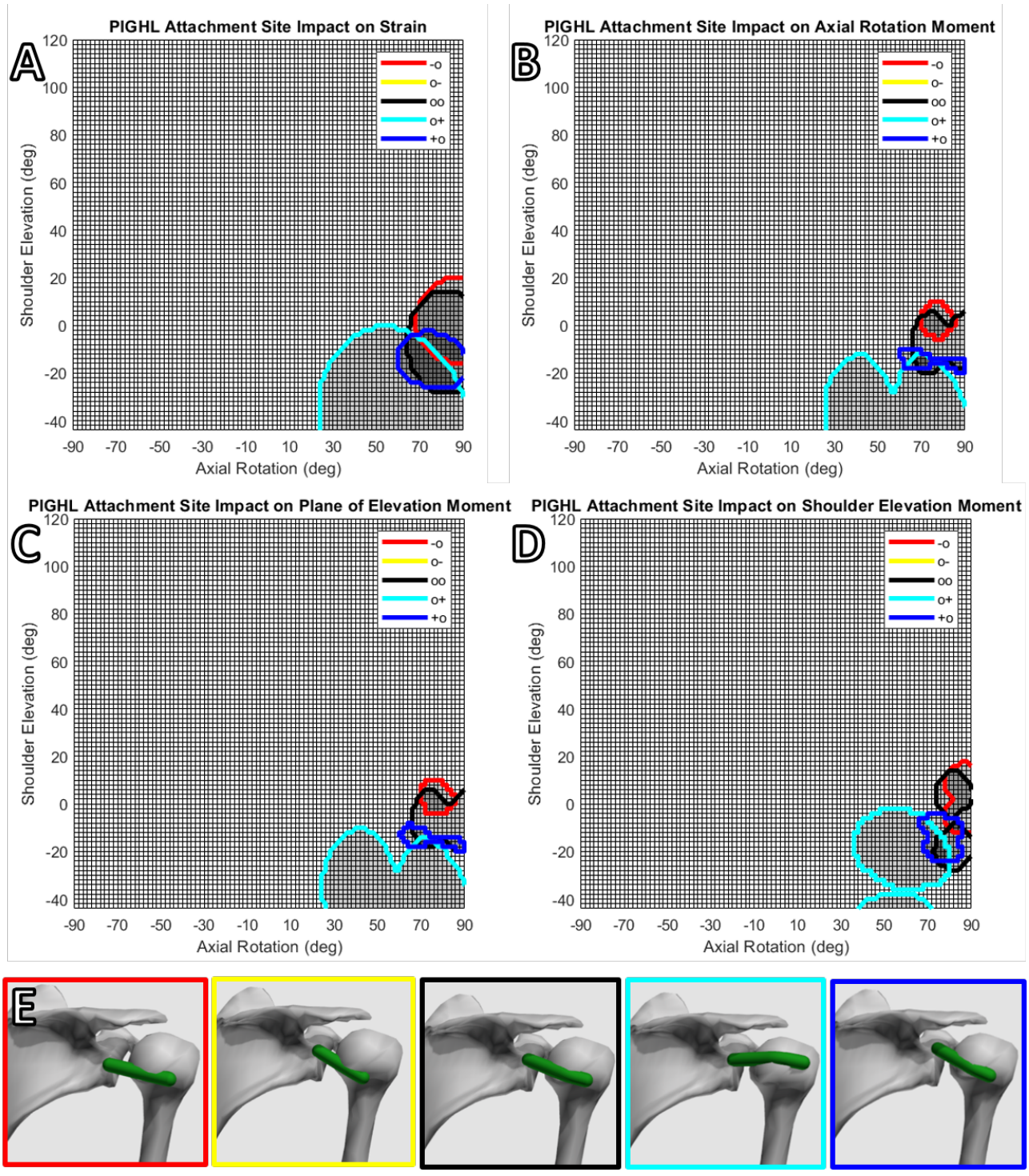

Figure 15: Impact of PIGHL attachment site variation on the range of motion. A shows the strain map, using 5% strain as the border. B, C and D show moment maps for axial rotation, plane of elevation and shoulder elevation respectively, using 1 Nm as border. E shows the different configurations in the model

In fig. 15 it shows the PIGHL limits the internal rotation when the arm is extended. Attaching to the lower bound on the humerus (o-) eliminates these limitations while attaching to the upper bound (o+) further limits the internal rotation, mainly while the arm is in extension.

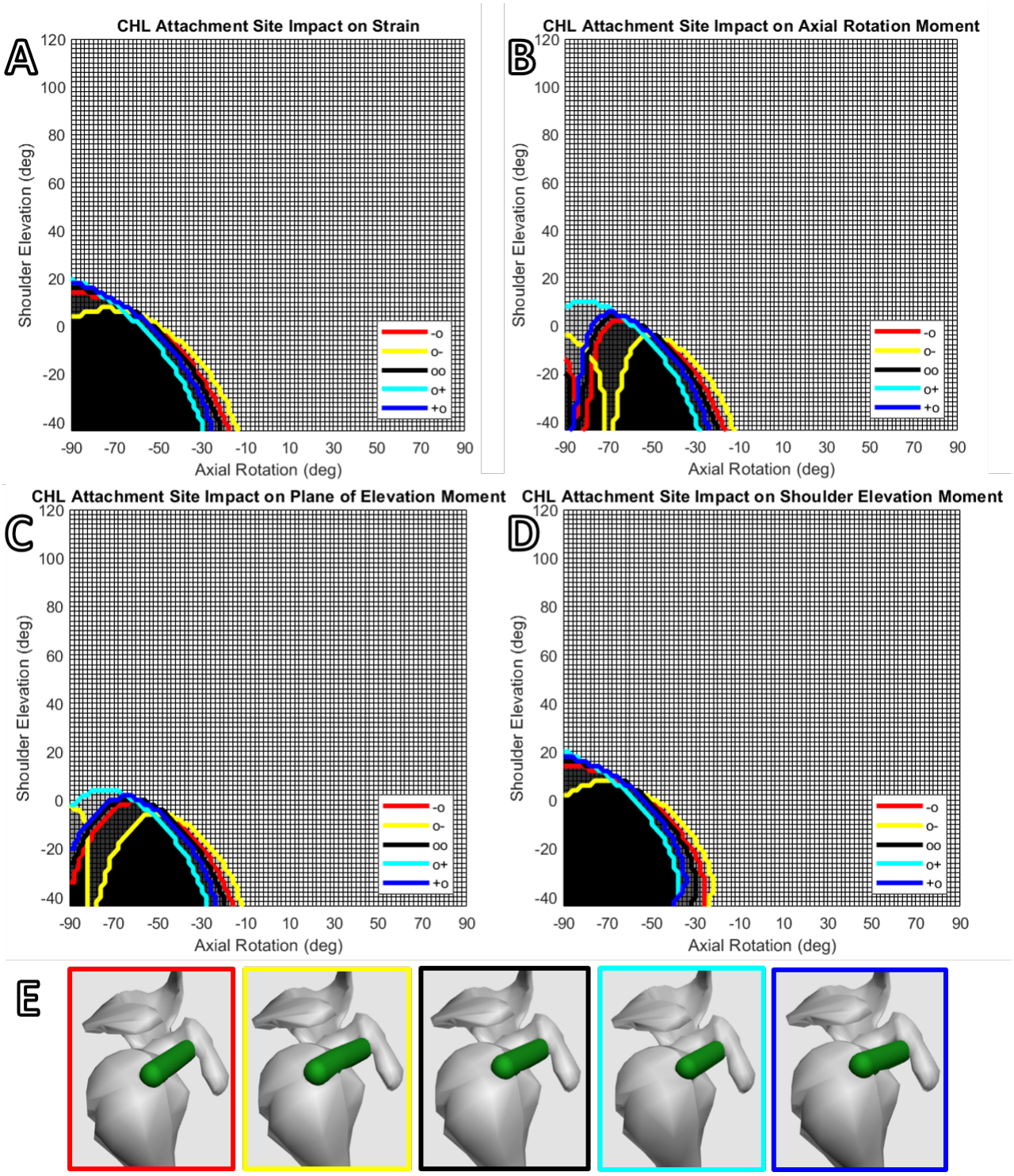

Figure 16: Impact of CHL attachment site variation on the range of motion. A shows the strain map, using 5% strain as the border. B, C and D show moment maps for axial rotation, plane of elevation and shoulder elevation respectively, using 1 Nm as border. E shows the different configurations in the model

The ROM limitations imposed by the CHL are comparable to those of the SGHL, mainly limiting shoulder extension and external rotation, as seen in fig. 16. Attachment to the lower bound on the humerus (o-) increases the limit on external rotation. However, the range of shoulder elevation for which external rotation is limited decreases. Attachment to the upper bound on the humerus (o+) decreases the limitation on external rotation.

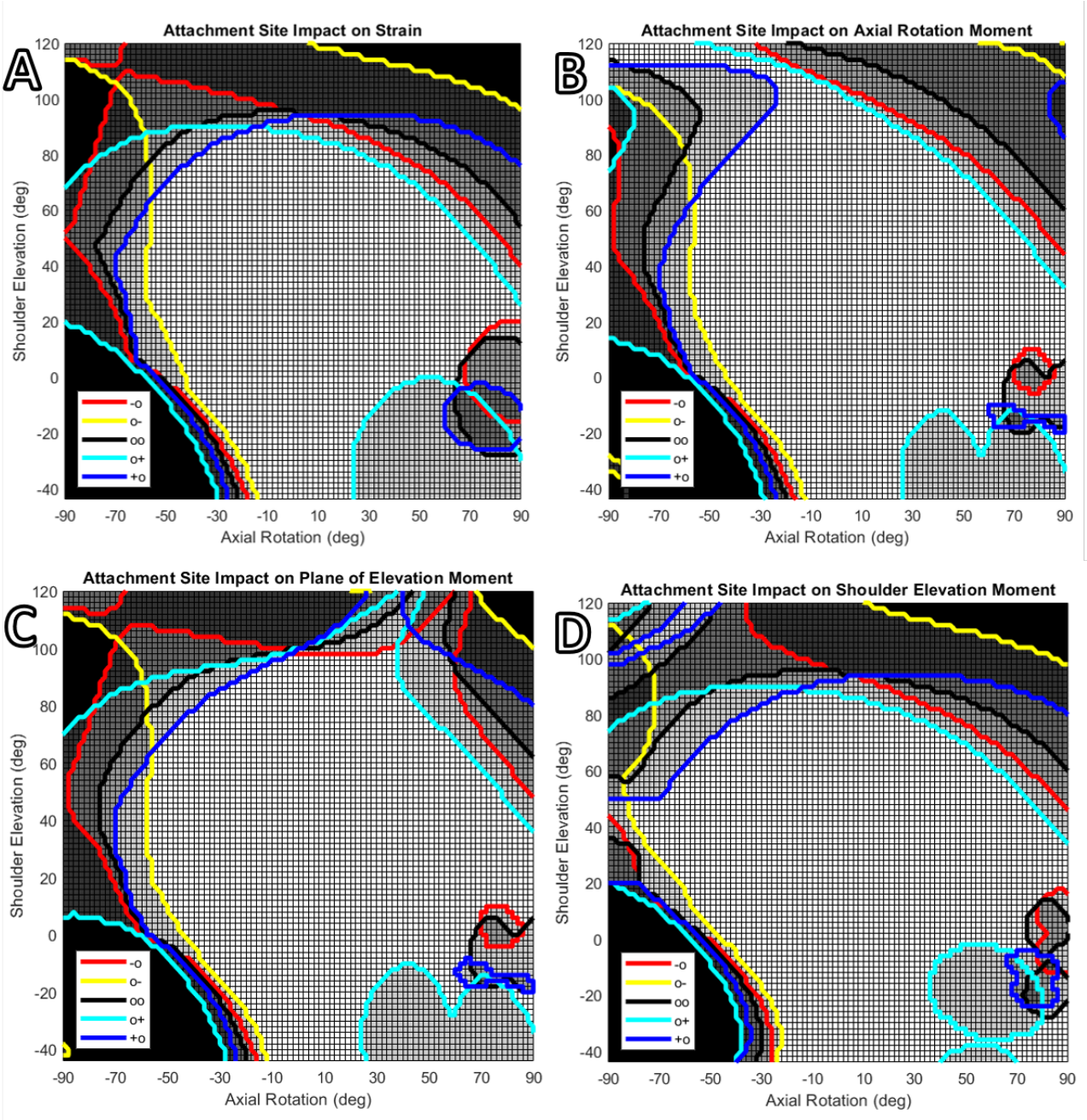

Figure 17: Impact of attachment site variation on the combined range of motion. A shows the strain map, using 5% strain as the border. B, C and D show moment maps for axial rotation, plane of elevation and shoulder elevation respectively, using 1 Nm as border.

Combining the strain maps and moment maps from the previous plots the overall effect on ROM is visualized in fig. 17. This shows attaching to the lower bound on the scapula (-o) results in more external rotation when shoulder elevation is positive and allowing for more shoulder elevation when the arm is externally rotated. On the other hand there is less internal rotation.

Attaching to the lower bound on the humerus (o-)removes the limitation on internal rotation and allows for more shoulder elevation, but limits the external rotation more.

Attaching to the upper bound on the humerus (o+) has the opposite effect, further limiting the internal rotation and shoulder elevation. Because the MGHL does not limit external rotation in this configuration it is not limited between 20° and 70° of shoulder elevation.

Lastly, attaching to the upper bound on the scapula (+o) results in more limitations on external rotation but allows for more internal rotation, with a similar limit on shoulder elevation.

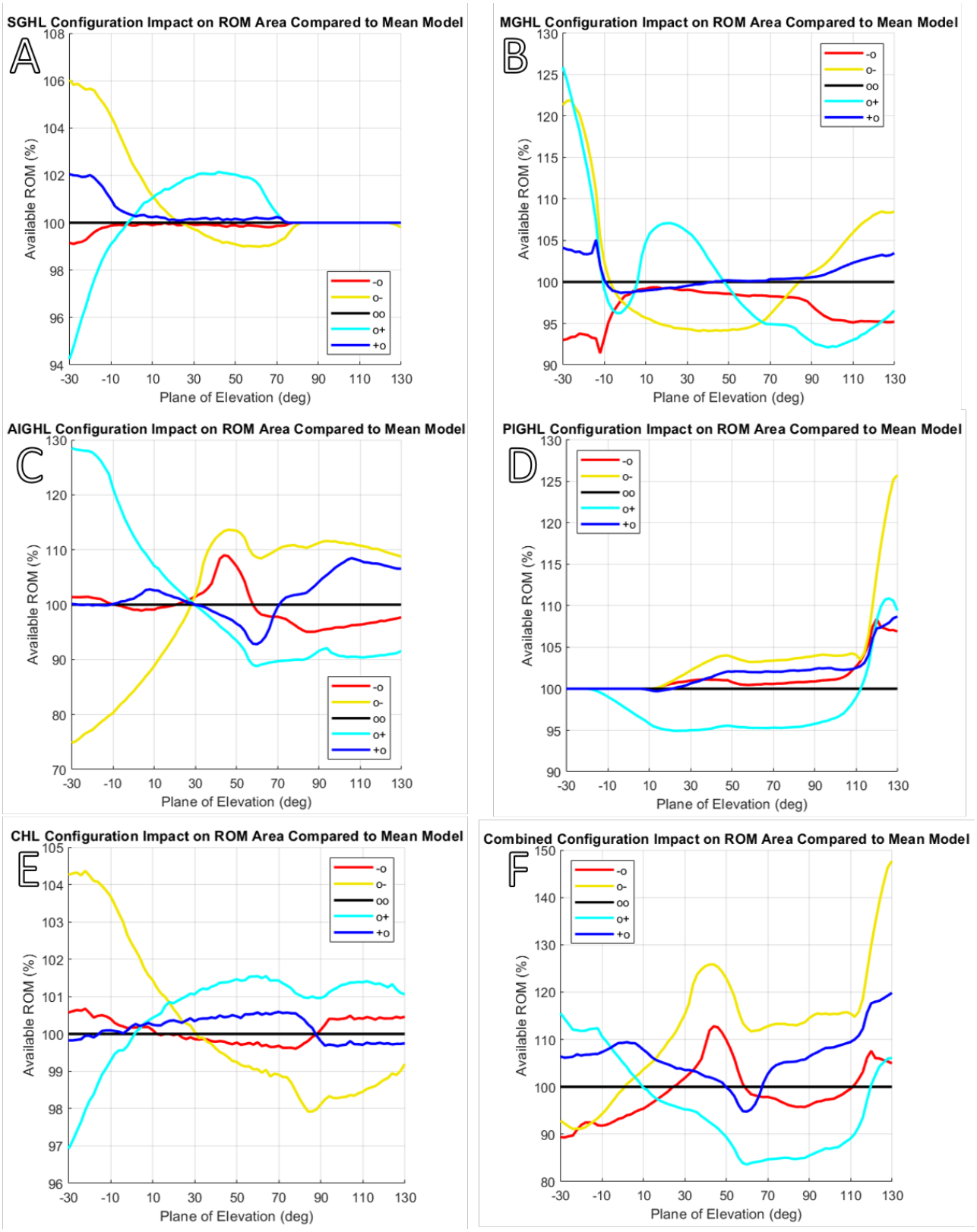

Figure 18: Relative changes in ROM area for different values of plane of elevation compared to the mean model (oo) for the SGHL(A), MGHL(B), AIGHL(C), PIGHL(D), CHL(E) and combined situation(F)

To analyze the impact of configuration changes on the ROM area for other values of the plane of elevation, fig. 18 shows graph of the area below the 5% strain border are shown as a percentage of the area produces by the mean configuration (oo). Looking at fig. 18 A, which shows the area below 5% strain for the different configurations as a percentage of the area of the mean configuration (oo), a similar pattern emerges for the other plane of elevation values, where the attachment of the scapula only has limited influence on the range of motion. On the other hand, changing the attachment on the humerus results in larger differences in the ROM.

Changing the humerus attachment from mean to the lower bound (o-) increases the range of motion for small and negative values of plane of elevation while losing some ROM for higher values. Changing the attachment to the upper bound (o+) has the opposite effect.

In fig. 18 B it appears that for both configurations with different humeral attachments (o- and o+), around 20 to 25% of ROM is gained near the lower limit of the plane of elevation.

As shown in fig. 18 C the mobility of the shoulder increases substantially for plane of elevation values below 30° if the attachment of the AIGHL on the humerus changes to the upper bound (o+). After this point, around 10% of the mobility is lost. The opposite is true for changing the attachment to the lower bound on the humerus (o-). Changing the attachment site on the scapula has less pronounced effects.

Looking at fig. 18 D it appears shoulder mobility is gained for plane of elevation values over 20° for most of the configurations. Notably, towards to upper limit of the plane of elevation, mobility is gained for all configurations. Having the ligament attach to the upper bound on the humerus (o+) limits the mobility across most of the planes of elevation.

The effect of attachment site variation on shoulder mobility is relatively low for the CHL as seen in fig. 18 E. Similar to the SGHL, attaching to the lower bound on the humerus (o-) gains some mobility for low and negative values of the plane of elevation but loses some for higher values. The opposite effect is seen for attaching to the upper bound on the humerus (o+).

The change in area for the combined effect of all ligaments for different configurations is shown in fig. 18 F. This shows that the o- and +o configuration gain ROM for most of the planes, whereas the o+ configuration loses ROM for most of the planes of elevation. Taking the average across all planes, the area for the -o configuration is 98.9% of the area of the oo configuration. For the o- configuration, this is 112.2%, for the o+ configuration 95.7% and for the +o configuration 106.2%.

3.2 Impact of length changes on range of motion

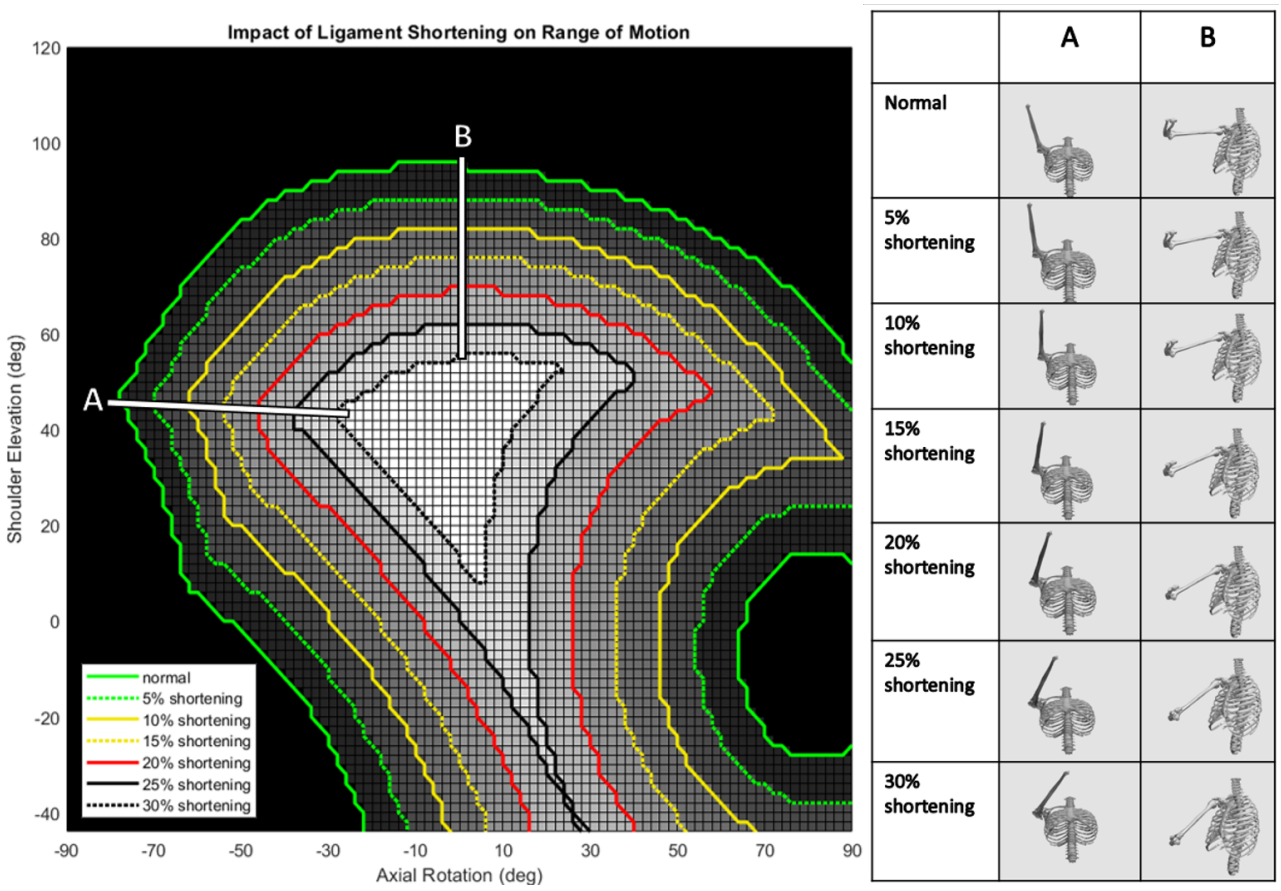

Figure 19: Strain map of the scaption plane for all ligaments. The poses of the model under A show the maximal external rotation in the scaption plane. The poses under B show the maximum shoulder elevation, which is at 0° axial rotation for all lengths.

Changing the rest length of the ligament alters the strain maps. In fig. 19 the shaded strain map in the scaption plane is shown for the healthy ligament, with a green line showing the 5% strain border. The other lines show

the 5% strain border for different levels of shortening, where the green dotted line depicts the border at 5% shortening, the yellow line at 10% shortening, the yellow dotted line at 15% shortening, the red line at 20% shortening, the black line at 25% shortening and the black dotted line at 30% shortening. Next to this shaded strain map, the model is depicted in different poses, where column A shows the maximum external rotation and column B shows the maximum shoulder elevation given the different rest lengths.

Shortening the ligaments by 5% increments appears to result in losing the outer border of the available space, where the thickness of the border remains fairly constant over the shortening steps. The thickness of the border does vary depending on the location, where the distance between the lines is smaller for negative axial rotation values, and larger for the positive numbers.

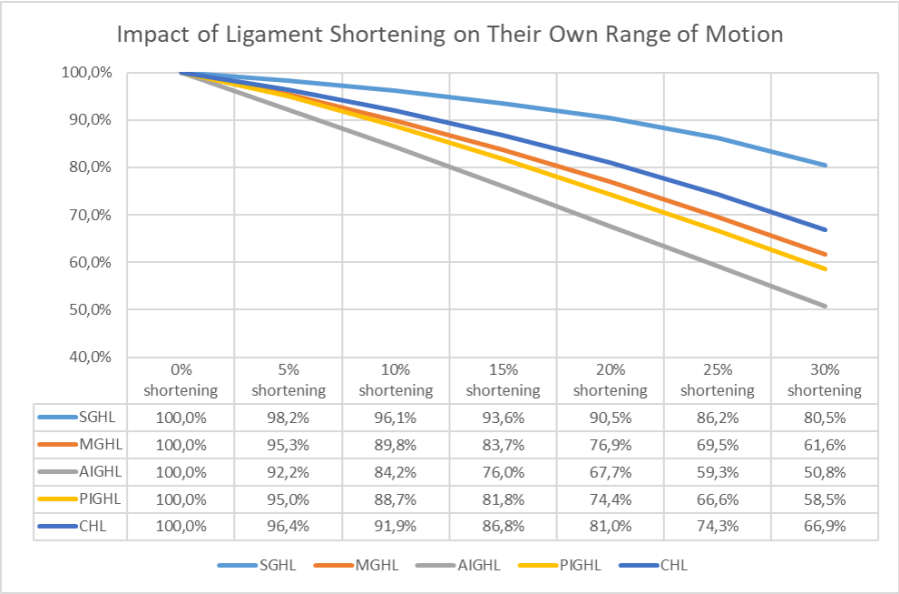

	0% shortening	5% shortening	10% shortening	15% shortening	20% shortening	25% shortening	30% shortening
SGHL	100,0%	98,2%	96,1%	93,6%	90,5%	86,2%	80,5%
MGHL	100,0%	95,3%	89,8%	83,7%	76,9%	69,5%	61,6%
AIGHL	100,0%	92,2%	84,2%	76,0%	67,7%	59,3%	50,8%
PIGHL	100,0%	95,0%	88,7%	81,8%	74,4%	66,6%	58,5%
CHL	100,0%	96,4%	91,9%	86,8%	81,0%	74,3%	66,9%

Figure 20: Impact of length changes on the availbe ROM determined by the ligaments.

The impact of shortening on the ROM as determined by individual ligaments is shown in fig. 20. The AIGHL is affected most by the shortening, having lost 50.2% of its ROM when 30% shortened. The PIGHL and MGHL show comparable results, loosing 41.5% and 38.4% of their available ROMs respectively. The CHL loses 33.1% of it ROM when shortened by 30% and the SGHL is least affected by shortening, only losing 19.5% of its ROM.

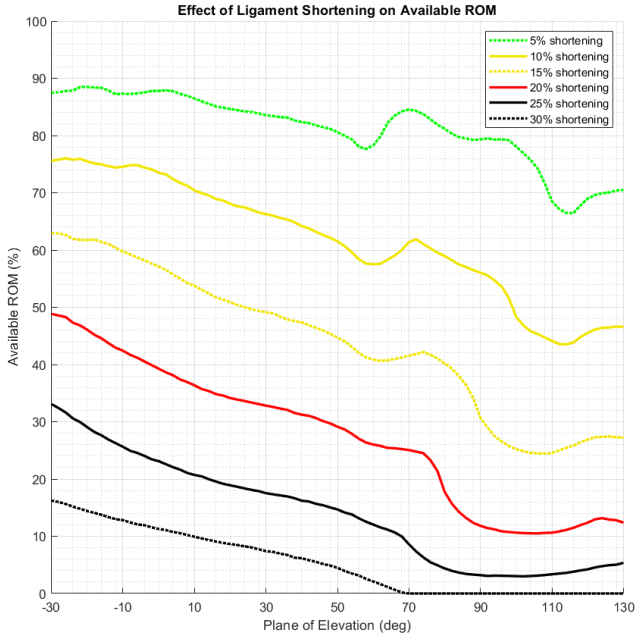

Figure 21: Figure shows the area of the range of motion as determined by the axial rotation and shoulder elevation as a percentage of the area in case of no shortening (healthy length) across the full range of motion for the plane of elevation.

Lastly, the area enclosed by the 5% strain border was calculated for each of the planes of elevation. This shows how shortening the ligaments does substantially influence the available range of motion. For 20% shortening there is at most 49% of the poses available compared to the healthy case, but when the plane of elevation exceeds 90° this is only around 12%. The average range of motion over all the planes of elevation is 81.2% for 5% shortening, 61.7% for 10% shortening, 43.8% for 15% shortening, 27.4% for 20% shortening, 14.0% for 25% shortening and 5.4% for 30% shortening.

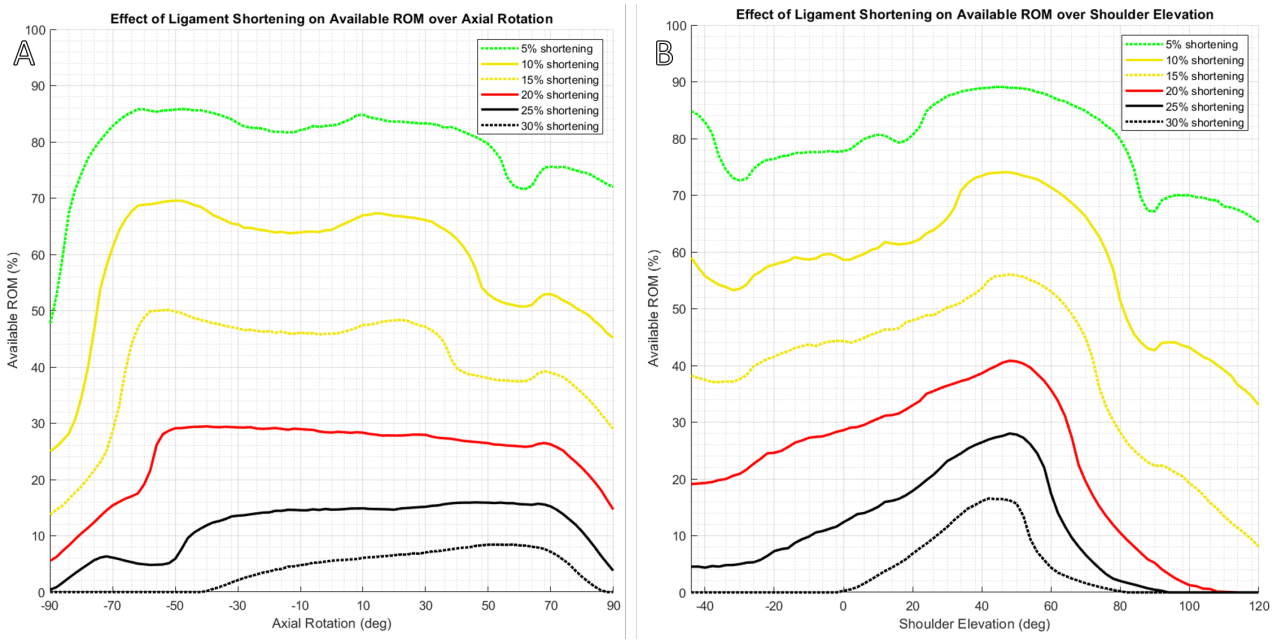

Figure 22: Figure shows the area of the range of motion as a percentage of the area in case of no shortening (healthy length) across the full range of motion for the axial rotation (A) and shoulder elevation (B).

The area of the ROM enclosed by the 5% strain margin is also plotted against the axial rotation and shoulder elevation angles in fig. 22 A and B respectively. This shows a steep drop towards the end range of external rotation, where only 50% of the area is left after 5% shortening. On the other end of the range, at large angles of internal rotation, there is also a drop in the available area. For values between 50° external and 50° internal rotation there seems to be a plateau, with a similar relative loss of area across that range. At larger amounts of shortening, this plateau shifts to the right, which appears to indicate that external rotation is affected more by shortening.

Looking at the area loss over shoulder elevation, it is the large angles of shoulder elevation where the largest relative changes occur. This is likely due to the limited initial size of the area. At 30% shortening, the model can no longer lower the shoulder below 0° or raise it above 80°.

Frozen shoulder is diagnosed by comparing the internal and external rotation and shoulder elevation to the unimpaired shoulder. A loss of 50% of these motions is set as the threshold for diagnosis. The effect of ligament shortening is on external rotation, shoulder elevation and internal rotation are shown in fig. 23 A, B and C respectively. The average percentages of the healthy motion that could be achieved for the different amounts of ligament shortening are shown in fig. 23 D. This shows that for 20% shortening the external and internal rotation have lost close to 50% of their range. For shoulder elevation this condition is only met when the rest length is shortened by 30%, mainly because the shoulder can no longer reach plane of elevation values over 70%.

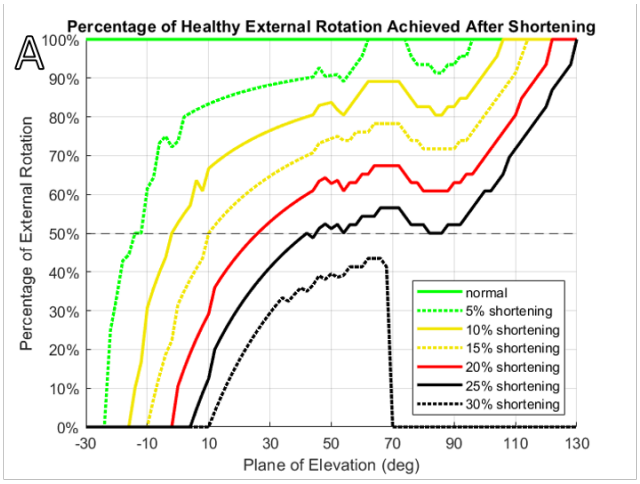

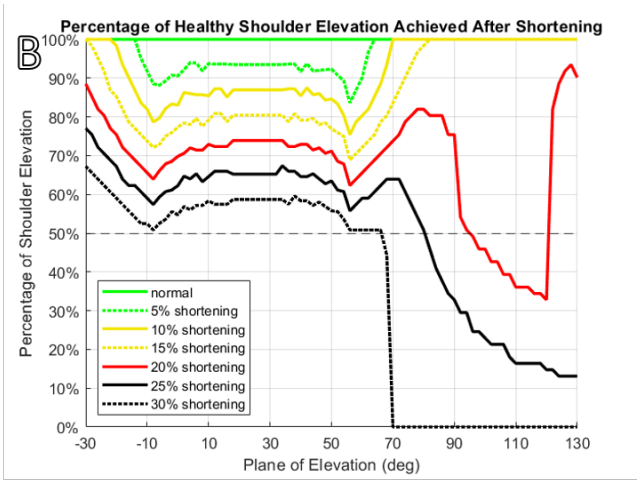

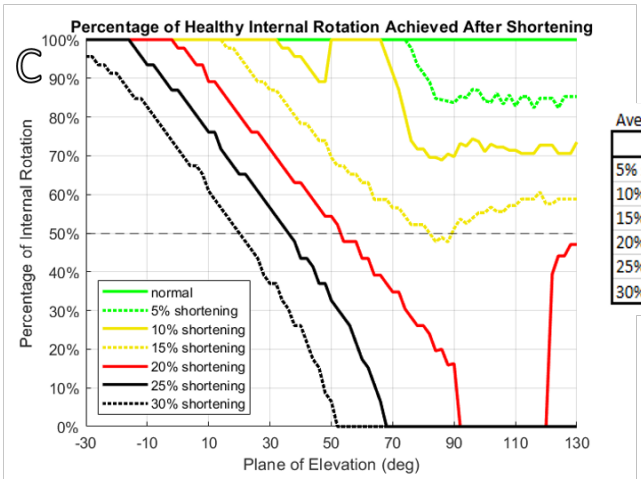

D

Average percentage of achievable movement compared to normal case

	External Rotation	Shoulder Elevation	Internal Rotation
5% shortening	83,1%	96,3%	95,1%
10% shortening	70,8%	91,9%	89,0%
15% shortening	60,5%	86,7%	75,3%
20% shortening	50,7%	68,2%	54,0%
25% shortening	41,4%	50,9%	39,3%
30% shortening	11,2%	34,9%	29,7%

Figure 23: A: Percentage of healthy external rotation that can be reached after rest length shortening. B: Percentage of healthy shoulder elevation that can be reached after rest length shortening. C: Percentage of healhty internal rotation that can be reached after rest length shortening. D: the average percentage of healthy motion that can be reached over all planes of elevation

3.3 Impact of stiffness changes on range of motion

The impact of stiffness change on the available range of motion is shown in fig. 24. The change for the axial rotation moment, plane of elevation moment and shoulder elevation moment are shown in fig. 24 A, C and E respectively. These graphs show the 1 Nm border for the normal situation as well as for the situation where the ligaments are 50% more stiff. In fig. 24 B, D and F the relative change in area is shown for the axial rotation moment, plane of elevation moment and shoulder elevation moment in that order. The solid green line shows the change for the normal case, the green dotted line for 10% stiffer ligaments, the yellow line for 20% stiffer ligaments, the yellow dotted line for 30% stiffer ligaments, the red line for 40% stiffer ligaments and the red dotted line for 50% stiffer ligaments.

Similarly to the changes due to shortening the largest relative differences can be found towards the extreme angles of that degree of freedom.

The impact of stiffness changes on the ROM of each of the individual ligaments is shown in fig. 25, as well as the combined impact the available ROM. The changes in the axial rotation moment, plane of elevation moment and shoulder elevation moment are shown in fig. 25 A, B and C respectively. The combined impact is similar for all three cases, but the contribution of the ligaments varies. The contribution for the SGHL is similar in all three cases. The PIGHL and CHL contribute more to the axial rotation and plane of elevation moment than to the shoulder elevation moment. The MGHL contributes more than the previously mentioned ligaments in all three cases. Its largest contribution is to the shoulder elevation moment. The AIGHL is impacted most by stiffness changes, mostly for the axial rotation and plane of elevation moments.

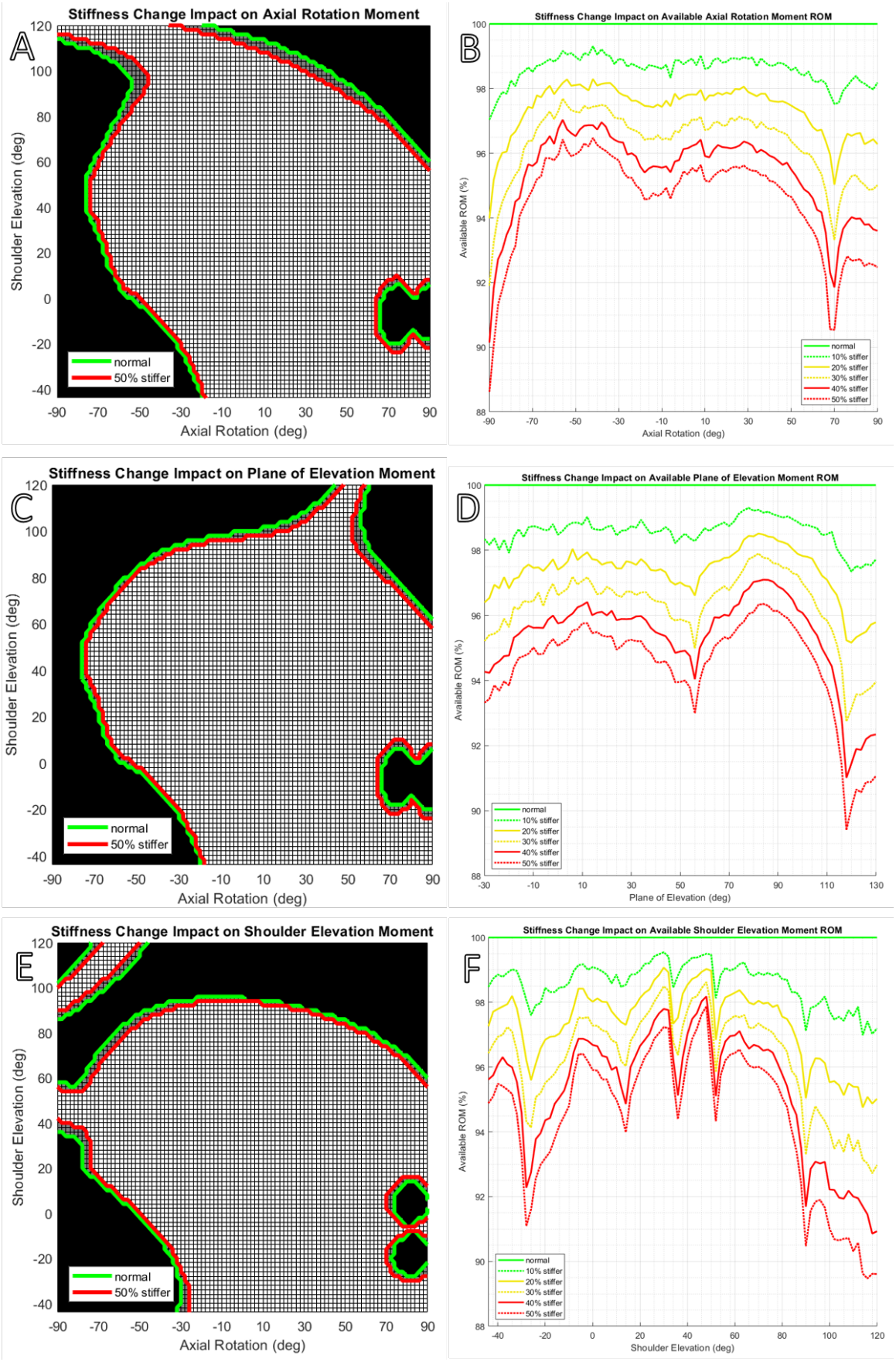

Figure 24: Shaded moment maps for the axial rotation moment, plane of elevation moment and shoulder elevation moment are shown for the scaption plane in figures A, C and E respectively. The green lines indicate the 1 Nm border as obtained with normal stiffness values. The red lines indicate the 1 Nm border as obtained by ligaments that are 50% more stiff. Figures B, D and F show the relative change in available ROM area caused by the increased stiffness for the axial rotation moment, plane of elevation moment and shoulder elevation moment respectively.

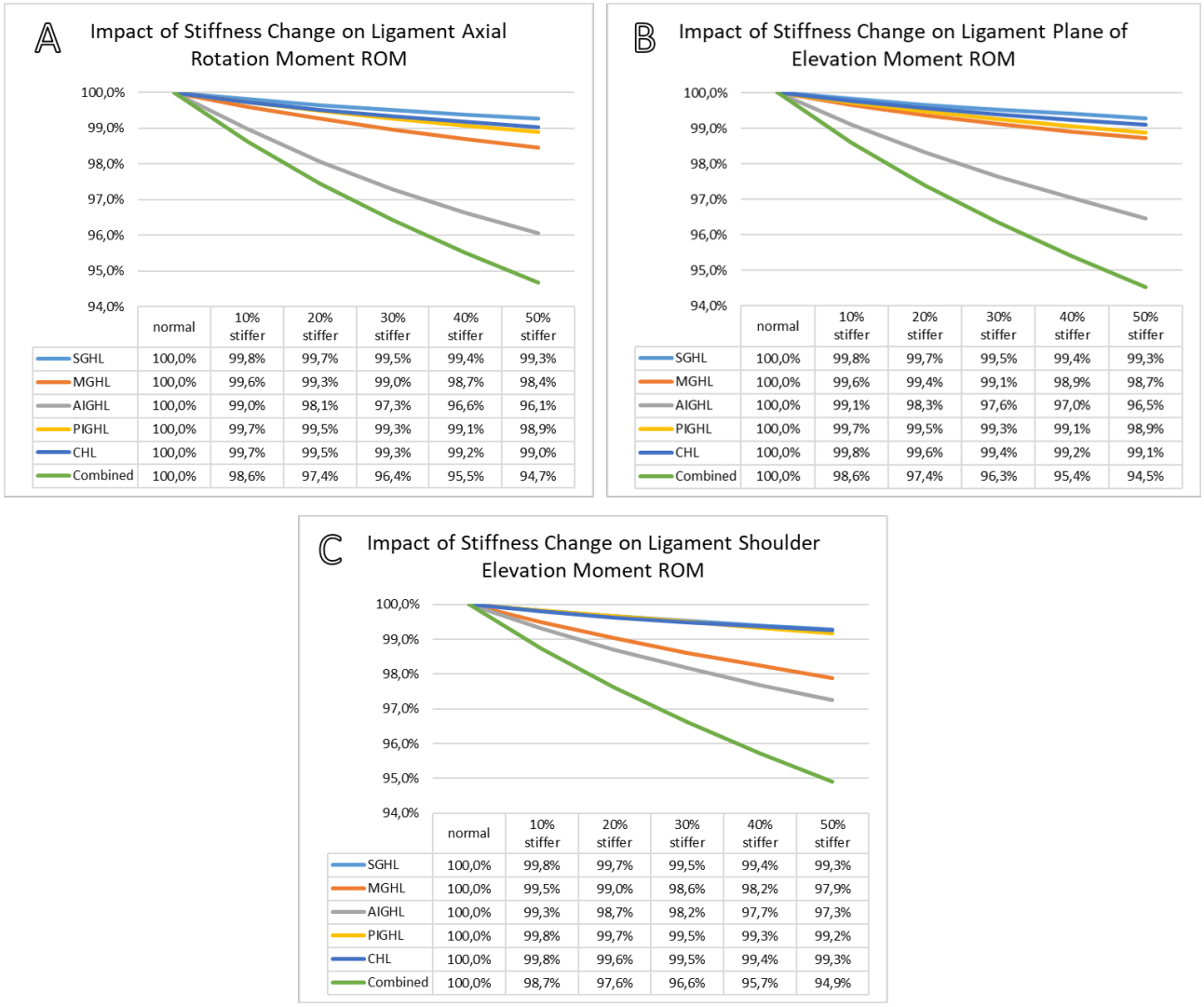

A	normal	10% stiffer	20% stiffer	30% stiffer	40% stiffer	50% stiffer
SGHL	100,0%	99,8%	99,7%	99,5%	99,4%	99,3%
MGHL	100,0%	99,6%	99,3%	99,0%	98,7%	98,4%
AIGHL	100,0%	99,0%	98,1%	97,3%	96,6%	96,1%
PIGHL	100,0%	99,7%	99,5%	99,3%	99,1%	98,9%
CHL	100,0%	99,7%	99,5%	99,3%	99,2%	99,0%
Combined	100,0%	98,6%	97,4%	96,4%	95,5%	94,7%

B	normal	10% stiffer	20% stiffer	30% stiffer	40% stiffer	50% stiffer
SGHL	100,0%	99,8%	99,7%	99,5%	99,4%	99,3%
MGHL	100,0%	99,6%	99,4%	99,1%	98,9%	98,7%
AIGHL	100,0%	99,1%	98,3%	97,6%	97,0%	96,5%
PIGHL	100,0%	99,7%	99,5%	99,3%	99,1%	98,9%
CHL	100,0%	99,8%	99,6%	99,4%	99,2%	99,1%
Combined	100,0%	98,6%	97,4%	96,3%	95,4%	94,5%

C	normal	10% stiffer	20% stiffer	30% stiffer	40% stiffer	50% stiffer
SGHL	100,0%	99,8%	99,7%	99,5%	99,4%	99,3%
MGHL	100,0%	99,5%	99,0%	98,6%	98,2%	97,9%
AIGHL	100,0%	99,3%	98,7%	98,2%	97,7%	97,3%
PIGHL	100,0%	99,8%	99,7%	99,5%	99,3%	99,2%
CHL	100,0%	99,8%	99,6%	99,5%	99,4%	99,3%
Combined	100,0%	98,7%	97,6%	96,6%	95,7%	94,9%

Figure 25: Impact of stiffness change on the available ROM determined by the ligaments. Figure A shows the impact on axial rotation moment, figure B on the plane of elevation moment and figure C on the shoulder elevation moment.

3.4 Impact of length, stiffness and attachment site changes on range of motion

After analyzing the impact of changing one parameter at a time, this section will present the effect of combining parameter changes on the available ROM.

In fig. 26 A the impact of length changes is shown for different configurations. Despite the differences in ROM area between these configurations, as seen in fig. 18 F, the results for the configurations with the same humeral attachments (-o, oo and +o) are very similar. The results for the models with different humeral attachments (o- and o+) differ more from the normal model. Having the ligaments attach to the upper bound on the humerus (o+) makes the model more susceptible to length changes. Attaching the ligaments to the lower bound on the humerus (o-) results in the smallest relative area loss.

The other three images in fig. 26, image B, C and D, show the effect of stiffness change on the ROM determined by the different moments for the different configurations. Similar to the length changes, the upper bound humerus attachments (o+) show the largest relative ROM loss, whereas the lower bound humerus attachments (o-) show the lowest relative ROM loss. The results of the lower bound scapula attachment configuration (-o) are very similar to the results of the mean model (oo). With the exception of the plane of elevation ROM, the -o configuration has a higher relative loss of area than the oo configuration.

The +o configuration has a lower relative loss than the oo configuration in all four of the cases. The difference is more pronounced for the stiffness changes than for the length changes.

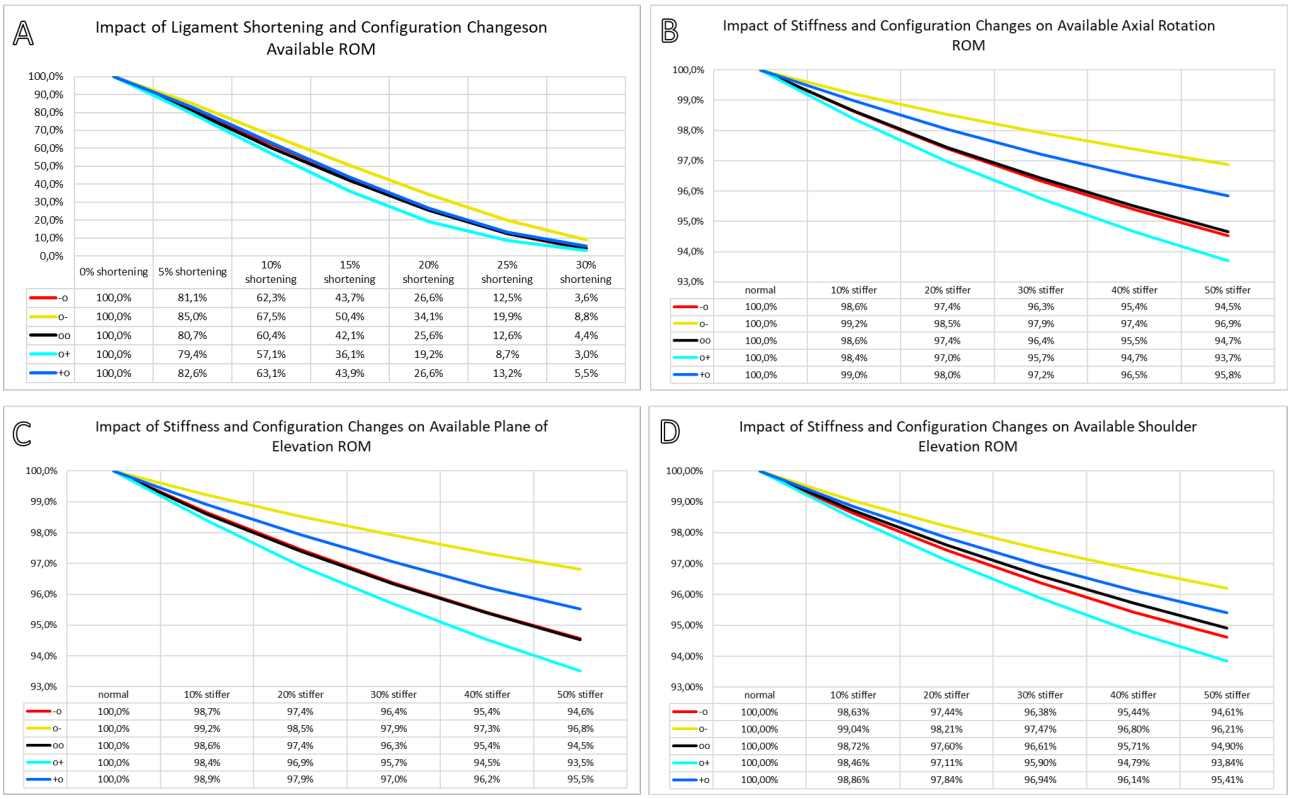

Figure 26: Image A shows the impact of length changes for different configurations. Images B, C and D show the impact of stiffness changes on the axial rotation moment ROM, plane of elevation moment ROM and shoulder elevation moment ROM for different configurations in that order.

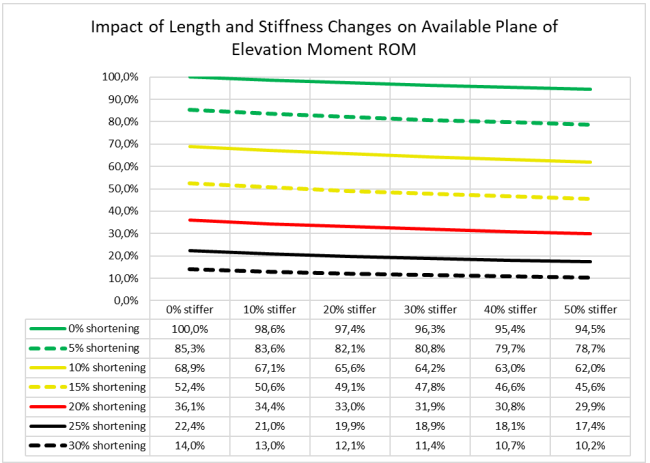

Figure 27: The impact of length and stiffness changes on the available ROM for the plane of elevation moment ROM

The effect of combining length and stiffness changes for the mean configuration (oo) is shown in fig. 27. This image shows that length changes result in the largest relative difference in range of motion. Shortening the rest length by 5% results in an ROM loss of 14.7%, whereas an increase in stiffness by 50% only results in a ROM loss of 5.5%. The slopes of these lines are -0.0108, -0.0132, -0.0137, -0.0135, -0.0122, -0.0099, -0.0075 in the order from 0% to 30% shortening. This shows the impact of stiffness changes is largest for the case of 10% shortening.

The effect of combining length and stiffness changes for different configurations is shown in fig. 28. Interesting to note is that the order that was seen in the other results, where the lowest relative change was attributed to the o- configuration and the largest relative change to the o+ configuration no longer holds when the ligaments are shortened by 25% or 30%. For these cases all other configurations have less relative ROM loss than the mean model (oo) except for the -o configuration. A similar pattern also appears for the ROM determined by the axial rotation moment as seen in fig. 29. In this case the o+ configuration does stay below the oo configuration,

meaning it has a larger relative ROM loss. For the ROM loss determined by the shoulder elevation moment, as seen in fig. 30, the o+ configuration has the largest relative ROM loss for all levels of shortening. The difference here is so large that 15% shortening of the o+ configuration results in a similar relative ROM loss as 20% shortening for the o- configuration.

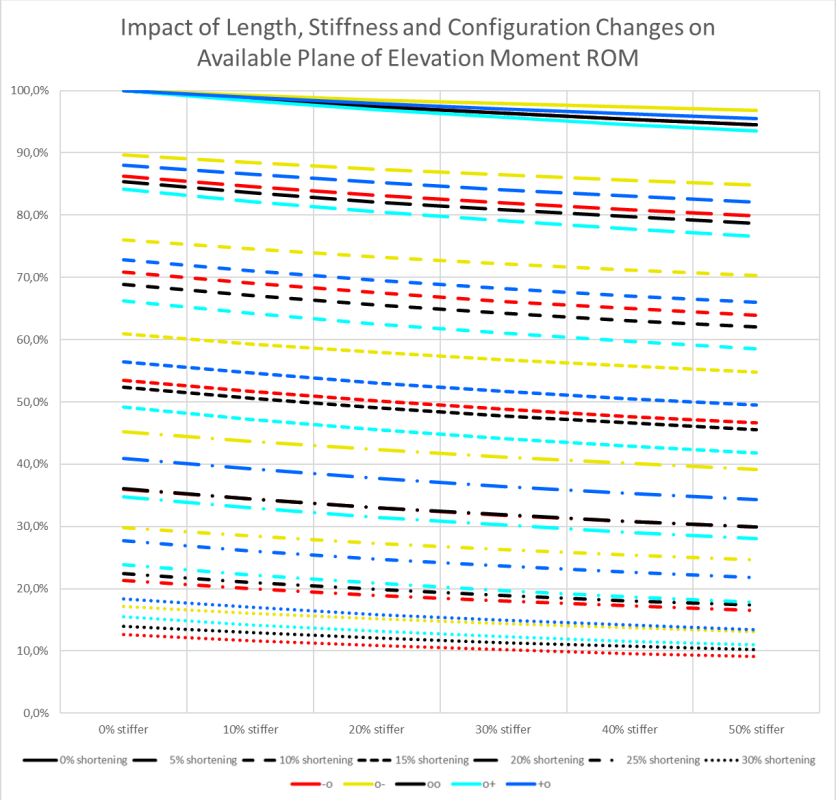

Figure 28: Graph showing the effect of length and stiffness changes on the relative ROM loss for different configurations. The ROM loss was analyzed for the plane of elevation moment with a boundary at 1 Nm.

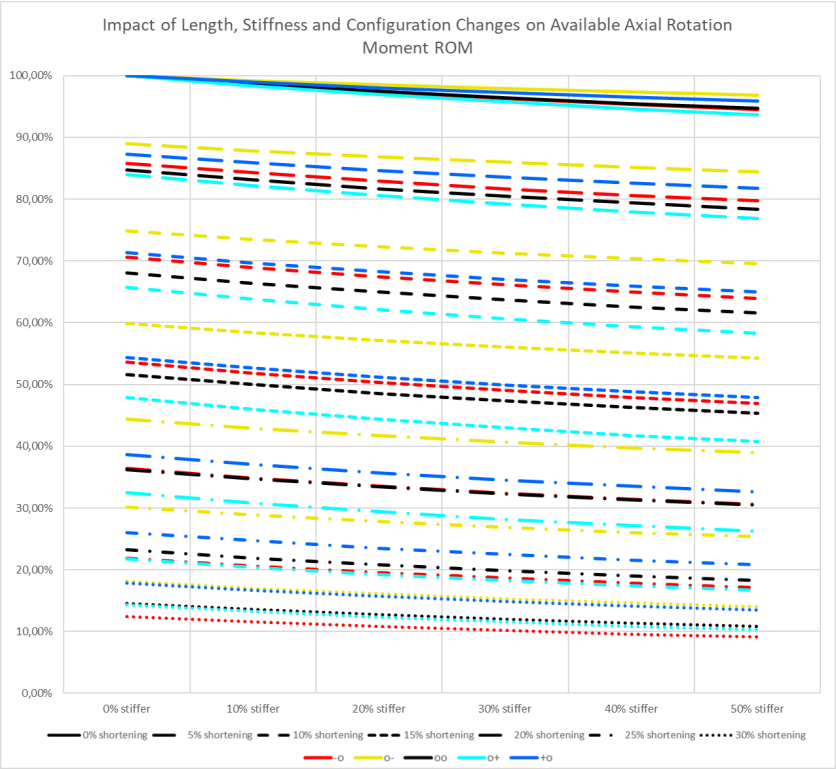

Figure 29: Graph showing the effect of length and stiffness changes on the relative ROM loss for different configurations. The ROM loss was analyzed for the axial rotation moment with a boundary at 1 Nm.

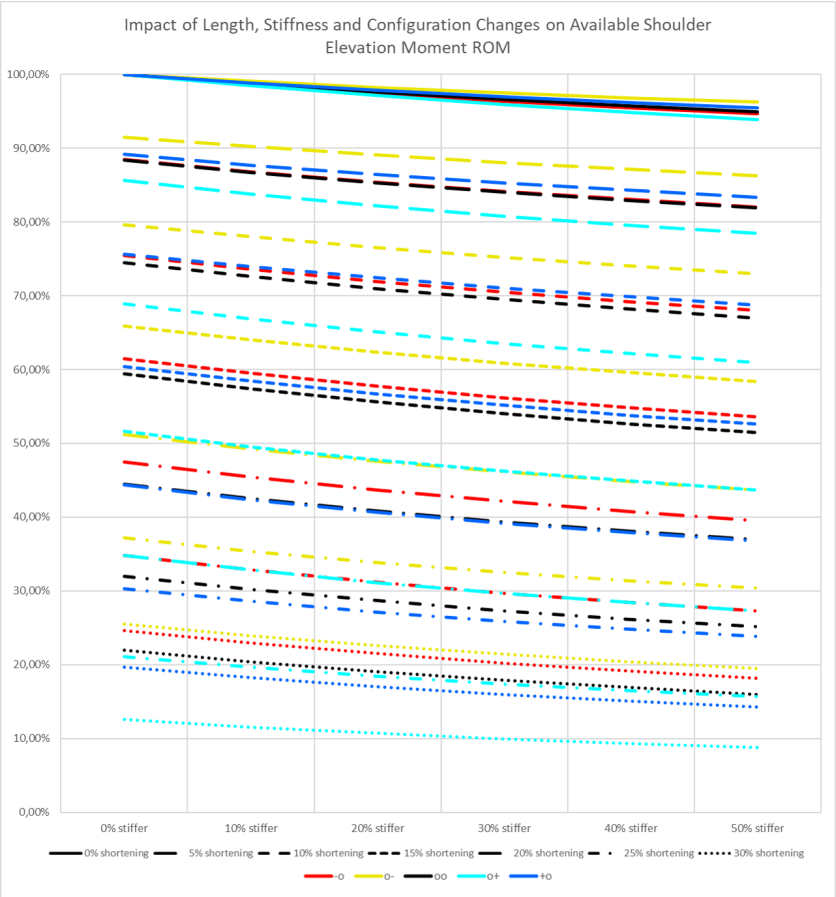

Figure 30: Graph showing the effect of length and stiffness changes on the relative ROM loss for different configurations. The ROM loss was analyzed for the shoulder elevation moment with a boundary at 1 Nm.

Average percentage of achievable movement compared to normal case

-o	External rotation	Shoulder elevation	Internal rotation
5% shortening	82,7%	96,0%	93,7%
10% shortening	71,7%	91,6%	86,4%
15% shortening	61,3%	86,3%	71,9%
20% shortening	51,5%	75,1%	50,6%
25% shortening	42,3%	52,7%	35,9%
30% shortening	14,3%	34,8%	24,9%

o-	External rotation	Shoulder elevation	Internal rotation
5% shortening	78,3%	98,6%	97,8%
10% shortening	62,9%	96,5%	94,9%
15% shortening	50,1%	94,0%	90,5%
20% shortening	39,9%	90,4%	82,4%
25% shortening	31,0%	60,8%	57,6%
30% shortening	22,5%	45,2%	47,8%

oo	External Rotation	Shoulder Elevation	Internal Rotation
5% shortening	83,1%	96,3%	95,1%
10% shortening	70,8%	91,9%	89,0%
15% shortening	60,5%	86,7%	75,3%
20% shortening	50,7%	68,2%	54,0%
25% shortening	41,4%	50,9%	39,3%
30% shortening	11,2%	34,9%	29,7%

o+	External rotation	Shoulder elevation	Internal rotation
5% shortening	93,0%	95,8%	92,6%
10% shortening	84,7%	90,9%	85,2%
15% shortening	73,0%	85,1%	65,6%
20% shortening	55,5%	76,7%	48,4%
25% shortening	31,3%	49,8%	30,4%
30% shortening	19,1%	37,6%	20,3%

+o	External rotation	Shoulder elevation	Internal rotation
5% shortening	83,2%	96,8%	99,2%
10% shortening	70,3%	92,7%	97,9%
15% shortening	59,5%	87,1%	95,6%
20% shortening	50,0%	77,7%	86,7%
25% shortening	40,6%	54,5%	67,0%
30% shortening	13,8%	40,8%	54,1%

Figure 31: Average percentage of healthy motion that can be reached over all planes of elevation for the different configurations

Lastly, the effect of rest length shortening on external and internal rotation and shoulder elevation, as seen in fig. 23, was analyzed for the different configurations. The average percentages are shown in fig. 31. It appears that configurations with the mean humeral attachment (-o, oo and +o) are most affected in external rotation. The o- and +o configurations are well protected against loss of internal rotation, where 30% shortening will result in only 52.2% and 45.9% loss of internal rotation, compared to 71.3% to 79.7% for the other configurations. Shoulder elevation remains relatively well preserved regardless of the configuration, where only the o+ configurations lowers it below 50% at 25% shortening.

4 Discussion

The aim of this study was to find the changes in ligament rest length and stiffness that were needed to induce the loss of range of motion as seen in frozen shoulder. Looking at the individual movements, shortening the rest lengths by 20% is enough for some of the configurations to cause a loss of 50% of external and internal rotation, which can be seen in fig. 31. Losing 50% of the shoulder elevation requires more shortening, with only one of the five configurations (o+) achieving this at 25% shortening. Three other configurations are close to 50% shoulder elevation loss at 25% (-o, oo and +o). Looking at fig. 27 a combination of 25% shortening and a stiffness increase of up to 50% could be enough to bring the shoulder elevation loss below 50% for these configurations as well.

A more robust approach that is less sensitive to modeling decisions is looking at the ROM area that is lost across the planes of elevation. If both axial rotation and shoulder elevation lose 50% of the range on both sides, this would leave an area of 25% of the original area. Looking at fig. 21, 20% shortening results in a loss of area of 72.6%. An increase in stiffness could bring this area loss to over 75%. If only shoulder flexion is assumed to

be affected and shoulder extension is not, an area loss of 68.75% would suffice. This condition can be met by only the 20% shortening of the rest length.

4.1 Discussion of the results

Given that the spread in attachment sites for all ligaments are larger on the humerus than on the scapula, combined with the greater size of the attachment ring compared to the glenoid, the distance between the attachment sites is larger on the humerus. This could explain why the scapular attachment appears to be of less influence on the range of motion compared to the variations in humerus attachment sites.

The spread in attachment sites for the AIGHL is relatively large on both the humerus and scapula, which could explain why the borders are further apart in fig. 14.

The effect of stiffness changes on the available range of motion was less pronounced than for the length changes. These results can be expected looking back at fig. 10 and fig. 11. The point at which the ligament starts to strain does not change, so the change in area is determined by the strain at which the ligaments reach the threshold of 1 Nm. As stated in the method this happens between 4.0% and 6.9% strain for the normal strain values and between 3.2% and 5.1% strain when the stiffness is increased by 50%.

The rest length of the ligaments was determined in such a way that the available ROM matches the data that was found in literature. As a result, the percentage of lengths that exceed the rest length, i.e. the area under the curve to the right of the vertical line in fig. 9 differs greatly between the ligaments. This area is directly correlated to the initial available range of motion. If the number of poses for which the ligament length exceeds the rest length is low, i.e. a small area under the curve to the right of the rest length, the available ROM will be large. If the physical changes due to shortening of the rest length are similar, for instance removing 5° from the border of the ROM, this will result in a larger relative impact for ligaments that started with smaller available ROMs. This could explain why the AIGHL was most susceptible to length changes as seen in fig. 20. This could also explain why the o- configuration showed lower relative ROM loss than the other models. This configuration has a larger initial ROM area, as seen in fig. 18 F, which would make the relative change lower. On the other hand, the o+ configuration has the smallest initial ROM and showed the most relative ROM loss, for instance when looking at fig. 26 A. The percentage of poses for which the rest length is exceeded for the different ligaments at different configurations is shown in fig. 32 B.

A

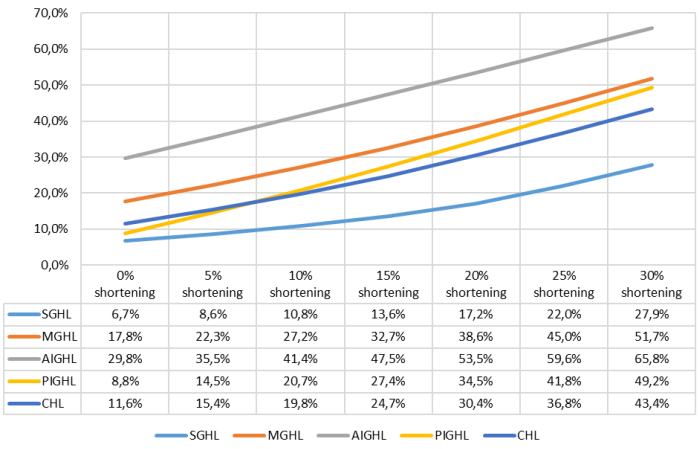

	0% shortening	5% shortening	10% shortening	15% shortening	20% shortening	25% shortening	30% shortening
SGHL	6,7%	8,6%	10,8%	13,6%	17,2%	22,0%	27,9%
MGHL	17,8%	22,3%	27,2%	32,7%	38,6%	45,0%	51,7%
AIGHL	29,8%	35,5%	41,4%	47,5%	53,5%	59,6%	65,8%
PIGHL	8,8%	14,5%	20,7%	27,4%	34,5%	41,8%	49,2%
CHL	11,6%	15,4%	19,8%	24,7%	30,4%	36,8%	43,4%

B

Percentage of poses for which the length exceeds the rest length

	SGHL	MGHL	AIGHL	PIGHL	CHL
-o	6,8%	20,6%	30,2%	7,4%	11,4%
o-	6,3%	17,0%	27,4%	4,4%	12,3%
oo	6,7%	17,8%	29,8%	8,8%	11,6%
o+	6,2%	19,6%	30,8%	10,8%	10,2%
+o	6,6%	16,7%	28,5%	7,1%	11,5%

Figure 32: Image A shows the impact of rest length shortening on the percentage of poses where the rest length is exceeded. Image B shows a table with the initial percentages of poses exceeding the rest length for different configurations.

Apart from the differences in area under the curve to the right of the rest length, the shape of the curve also plays a role in the ligaments susceptibility to length changes. In fig. 32 A the effect of rest length shortening on the percentage of poses for which the rest length is exceeded is shown for the different ligaments. Looking at fig. 9 A through E there is a tail towards the upper end of the lengths. This is not the case for the PIGHL. Furthermore, a larger rest length will have a larger absolute change due to shortening (10% shortening leads to a 0.00429 shorter MGHL rest length but a 0.00632 shorter PIGHL rest length). Combining this explains why the percentage of poses that exceeds the rest length is almost equal for the PIGHL and MGHL at 30%

shortening despite the large initial difference. This could also explain the phenomenon described in section 3.2, where more ROM area appeared to be lost on the PIGHL side than the MGHL side.

Using the mean length over all the poses to determine the scaling factor for the rest length was the preferred method as this is less sensitive to outliers. Different methods, like using the difference between the largest and smallest length, would have resulted in similar scaling factors for most configurations, but for some configurations would have resulted in differences in rest length of up to 14%.

Although the rest lengths were scaled for different configurations, no changes were made to the stiffness values between configurations. The articles from which the stiffness values were retrieved based them on average values. For this reason the same values were applied to all configurations. Future research should aim to find ligament stiffness values for different configurations.

In the current study configuration changes were applied to all ligaments. For instance, in the o+ model, all ligaments were attached to the upper bound on the humeral attachment site. Using the five described configurations, a total of 3125 combinations could be made, but only five of them were explored.

Some studies provided data on how often a certain attachment site was found, for instance Itoigawa et al stating the AIGHL attached between 4 and 5 'o-clock in 2% of the case [29]. Only one study reported on humeral attachment sites [21]. However, no articles were found to describe how often combinations of certain glenoid and humerus attachments were found. As a result, it is unknown if an o+ configurations is equally likely as an o- configuration, or if they exist. Given the impact the humeral attachment has on the range of motion, as found in this study, future research should aim to analyze the humerus attachments and the combinations of glenoid and humerus attachments.

The fact that the slope of the curve was largest for the case of 10% shortening in fig. 19 could be explained by the fact that the length of the border is longest for that case, as the change in ROM due to stiffness changes occurs near that strain border.

4.2 Limitations

Due to instabilities in the wrapping algorithm, the radii of the wrapping surfaces could not be maintained for the different configurations. This will have influenced the ligament lengths as well as the moment arms. The change in length due to a different wrapping surface was limited by scaling the rest lengths based on the ligament lengths but it is difficult to determine how much of the error could be remedied this way. The wrapping surfaces used were ellipsoids with an X, Y and Z radius. They were often different from each other, and because the moment arms are strongly dependent on the way the ligament wraps around this ellipsoid, it was not feasible to limit these errors once the data was collected. The radii of the wrapping surfaces used in the models as well as some examples of the issues that occurred can be found in Appendix A. Future research would benefit from a stable wrapping algorithm so the radii can be kept constant for different configurations.

Detailed information on the available range of motion for the glenohumeral joint was sparse. Only a few articles provided information on some of the achievable end poses. This information was needed to determine the rest length of the ligaments, as these are supposed to strain towards the end of the range of motion. Having more data points would allow for a better estimation of the rest lengths.

Information on the available range of motion for the glenohumeral joint in the case of frozen shoulder could not be found. This data would have been extremely helpful to determine how closely the impaired range of motion in frozen shoulder could be recreated with length, stiffness and configuration changes. The described diagnostic requirement of a loss of 50% of the external and internal rotation and shoulder elevation do not specify for which poses this is measured. At 0° plane of elevation 50% of external rotation was lost by shortening the rest length by 10%. For higher angles of plane of elevation this condition was no longer met with this amount of shortening, and for the scaption plane (40° plane of elevation) the ligament rest length would require 25% shortening to meet this condition. If the condition of losing 50% of the external rotation only needs to hold for a few poses it can be achieved with relatively small changes. If it needs to hold for all the planes of elevation this would only be met by shortening the ligament rest length by 30%.

Future research should aim to obtain more detailed data on the available range of motion for the glenohumeral joint. This could be done using one or more cadavers in combination with a robotic system that could apply a set torque and measure the angles at which the limit is reached.

Most of the data on the range of motion regarded the ROM in the scaption plane. As a result, the ligament rest lengths were tuned to closely match this data in the scaption plane. However, for different planes of elevation, this could lead to ranges of motion that seem unrealistic. Many of these issues were caused by the PIGHL, which could be subjected to high levels of strain for poses ranging from internal rotation and shoulder

extension to external rotation and shoulder flexion. This would cause the ROM area to be cut diagonally. An example of this can be seen in fig. 33. A balance needed to be found between increasing the rest length to the point where the ROM area was no longer cut in half and not increasing the rest length so much that the ligament no longer prevented the model from reaching certain poses. This effect is also the cause of the sharp jumps in the graphs of fig. 23 B and C. More detailed information on the range of motion would provide insight in how to balance this better.

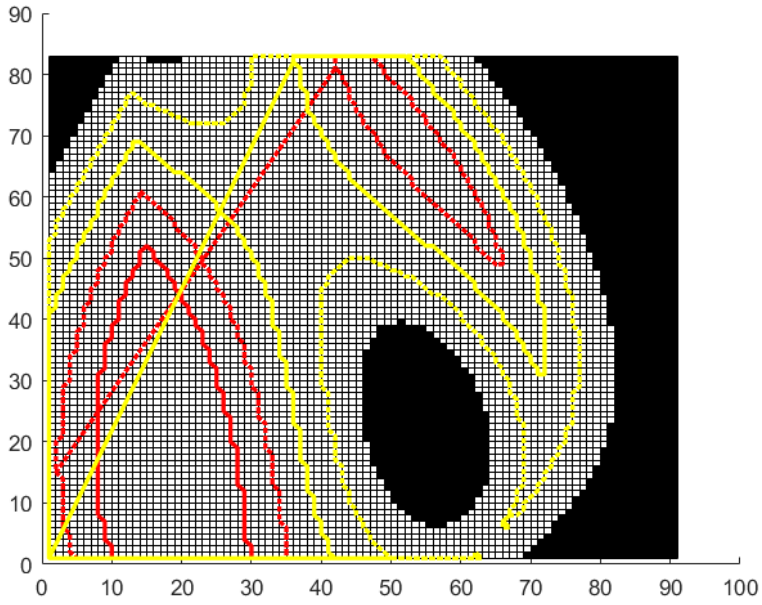

Figure 33: This image shows how the range of motion area is cut in half due to ligament rest length shortening

Another limitation is the simplification process that was used to create the model. In reality the glenohumeral joint capsule is more complex than just these five lose ligaments. There is a trade-off between closely recreating the complex anatomy of the shoulder joint and computational efficiency. To determine if the simplifications made for these models are justified the results should be validated. This could be done using cadavers where the torque required for a certain motion is measured. Making a change to the joint capsule, for instance cutting one of the ligaments to eliminate its contribution, this experiment should be repeated and compared to the results from the model if that same ligament is ignored.

Given the capsule loops around the full joint surface, stretching the capsule on one side would lead to compression of the capsule on the other side. In the current models, the ligaments were assumed to be stretch-only springs, where a force was only exerted if the ligaments were stretched. It is not unthinkable that increasing the stiffness of the capsule would cause a higher joint torque as more force is required to buckle the capsule. This could also be measured using cadavers by cutting the part of the capsule that would buckle and see if there is a difference in force required to move the joint. For the model this could mean that the impact of stiffness changes on the available ROM increases.

Finally, no articles were found to quantify the length changes that the ligaments undergo in frozen shoulder. Future research should aim to quantify the relative change in length of these ligaments, for instance by comparing the ligament lengths to those of the healthy shoulder. This information would put the results of this study in perspective, to see if 20% shortening does indeed occur.

5 Conclusion

Using these models, the effect that structural changes in ligaments have on the range of motion can be analyzed. This can be used to study how the ROM is affected by structural changes like length and stiffness changes that are associated with frozen shoulder.

Ligament lengths are believed to change in frozen shoulder. Changes in ligament length in the model have large effects on the available ROM, limiting axial rotation on either side as well as shoulder elevation. Although these degrees of freedom were limited by over 50% for parts of the range of the plane of elevation, this could

not be said for the full range. Averaging the values over the full range, the conditions were met for 20 to 25% shortening.

Stiffness changes are also associated with frozen shoulder. The effects of ligament stiffness changes on the joint moment can be analyzed using these models.

Although frozen shoulder will not change the attachment sites of the ligaments, models with different configurations could be used in an attempt to find ligament configurations that are more likely to develop frozen shoulder.

References

[1] M. J. Kelley, P. W. Mcclure, and B. G. Leggin, "Frozen shoulder: evidence and a proposed model guiding rehabilitation," *Journal of orthopaedic & sports physical therapy*, vol. 39, no. 2, pp. 135–148, 2009.

[2] E. Maund, D. Craig, S. Suekarran, A. Neilson, K. Wright, S. Brealey, L. Dennis, L. Goodchild, N. Hanchard, A. Rangan *et al.*, "Management of frozen shoulder: a systematic review and cost-effectiveness analysis," 2012.

[3] B. Reeves, "The natural history of the frozen shoulder syndrome," *Scandinavian journal of rheumatology*, vol. 4, no. 4, pp. 193–196, 1975.

[4] A. Aydeniz, S. Gursoy, and E. Guney, "Which musculoskeletal complications are most frequently seen in type 2 diabetes mellitus?" *Journal of International Medical Research*, vol. 36, no. 3, pp. 505–511, 2008.

[5] J. Bridgman, "Periarthritis of the shoulder and diabetes mellitus," *Annals of the rheumatic diseases*, vol. 31, no. 1, p. 69, 1972.

[6] B. J. Lundberg, "The frozen shoulder: clinical and radiographical observations the effect of manipulation under general anesthesia structure and glycosaminoglycan content of the joint capsule local bone metabolism," *Acta Orthopaedica Scandinavica*, vol. 40, no. sup119, pp. 1–59, 1969.

[7] B. Pal, J. Anderson, W. Dick, and I. D. Griffiths, "Limitation of joint mobility and shoulder capsulitis in insulin-and non-insulin-dependent diabetes mellitus," *Rheumatology*, vol. 25, no. 2, pp. 147–151, 1986.

[8] R. C. Manske and D. Prohaska, "Diagnosis and management of adhesive capsulitis," *Current reviews in musculoskeletal medicine*, vol. 1, pp. 180–189, 2008.

[9] T. Bunker, "Frozen shoulder: unravelling the enigma," *Annals of the Royal College of Surgeons of England*, vol. 79, no. 3, p. 210, 1997.

[10] N. Balci, M. K. Balci, and S. Tüzüner, "Shoulder adhesive capsulitis and shoulder range of motion in type ii diabetes mellitus: association with diabetic complications," *Journal of Diabetes and its Complications*, vol. 13, no. 3, pp. 135–140, 1999.

[11] E. Ahmad, S. Lim, R. Lamptey, D. R. Webb, and M. J. Davies, "Type 2 diabetes," *The Lancet*, vol. 400, no. 10365, pp. 1803–1820, 2022.

[12] H. Sun, P. Saeedi, S. Karuranga, M. Pinkepank, K. Ogurtsova, B. B. Duncan, C. Stein, A. Basit, J. C. Chan, J. C. Mbanya *et al.*, "Idf diabetes atlas: Global, regional and country-level diabetes prevalence estimates for 2021 and projections for 2045," *Diabetes research and clinical practice*, vol. 183, p. 109119, 2022.

[13] S. Jones, N. Hanchard, S. Hamilton, and A. Rangan, "A qualitative study of patients' perceptions and priorities when living with primary frozen shoulder," *BMJ open*, vol. 3, no. 9, p. e003452, 2013.

[14] K. L. Boyle-Walker, D. L. Gabard, E. Bietsch, D. M. Masek-VanArsdale, and B. L. Robinson, "A profile of patients with adhesive capsulitis," *Journal of hand therapy*, vol. 10, no. 3, pp. 222–228, 1997.

[15] J. Zuckerman, F. Cuomo, and S. Rokito, "Definition and classification of frozen shoulder: a consensus approach," *J Shoulder Elbow Surg*, vol. 3, no. 1, p. S72, 1994.

[16] G. Hand, N. Athanasou, T. Matthews, and A. Carr, "The pathology of frozen shoulder," *The Journal of Bone & Joint Surgery British Volume*, vol. 89, no. 7, pp. 928–932, 2007.

[17] Y. Terzi, K. Akgün, İ. AKTAŞ, D. Palamar, and G. Can, "The relationship between generalized joint hypermobility and adhesive capsulitis of the shoulder," *Archives of Rheumatology*, vol. 28, no. 4, pp. 234–241, 2013.

[18] A. Atici, İ. Aktas, P. Akpinar, and F. Unlu Ozkan, "The relationship between joint hypermobility and subacromial impingement syndrome and adhesive capsulitis of the shoulder," *Northern Clinics of İstanbul*, vol. 5, no. 3, pp. 232–237, 2018.

[19] K. J. Park, M. Tamboli, L. Y. Nguyen, M. H. McGarry, and T. Q. Lee, "A large humeral avulsion of the glenohumeral ligaments decreases stability that can be restored with repair," *Clinical Orthopaedics and Related Research®*, vol. 472, pp. 2372–2379, 2014.

[20] J. Chahla, Z. S. Aman, J. A. Godin, M. E. Cinque, M. T. Provencher, and R. F. LaPrade, "Systematic review of the anatomic descriptions of the glenohumeral ligaments: a call for further quantitative studies," *Arthroscopy: The Journal of Arthroscopic & Related Surgery*, vol. 35, no. 6, pp. 1917–1926, 2019.

[21] T. J. Dekker, Z. S. Aman, L. A. Peebles, H. W. Storaci, J. Chahla, P. J. Millett, and M. T. Provencher, "Quantitative and qualitative analyses of the glenohumeral ligaments: an anatomic study," *The American Journal of Sports Medicine*, vol. 48, no. 8, pp. 1837–1845, 2020.

[22] K. Kask, E. Põldoja, T. Lont, R. Norit, M. Merila, L. C. Busch, and I. Kolts, "Anatomy of the superior glenohumeral ligament," *Journal of shoulder and elbow surgery*, vol. 19, no. 6, pp. 908–916, 2010.

[23] J. Steinbeck, U. Liljenqvist, and J. Jerosch, "The anatomy of the glenohumeral ligamentous complex and its contribution to anterior shoulder stability," *Journal of shoulder and elbow surgery*, vol. 7, no. 2, pp. 122–126, 1998.

[24] N. Pouliart, K. Somers, and O. Gagey, "Arthroscopic glenohumeral folds and microscopic glenohumeral ligaments: the fasciculus obliquus is the missing link," *Journal of shoulder and elbow surgery*, vol. 17, no. 3, pp. 418–430, 2008.

[25] J. J. Warner, D. N. Caborn, R. Berger, F. H. Fu, and M. Seel, "Dynamic capsuloligamentous anatomy of the glenohumeral joint," *Journal of shoulder and elbow surgery*, vol. 2, no. 3, pp. 115–133, 1993.

[26] A. Alashkham, A. Alraddadi, and R. Soames, "Anatomy of the glenohumeral ligaments," *Italian Journal of Anatomy and Embryology*, vol. 123, no. 2, pp. 114–126, 2018.

[27] V. C. Eberly, P. J. McMahon, and T. Q. Lee, "Variation in the glenoid origin of the anteroinferior glenohumeral capsulolabrum." *Clinical Orthopaedics and Related Research (1976-2007)*, vol. 400, pp. 26–31, 2002.

[28] J. Ide, S. Maeda, and K. Takagi, "Normal variations of the glenohumeral ligament complex: an anatomic study for arthroscopic bankart repair," *Arthroscopy: The Journal of Arthroscopic & Related Surgery*, vol. 20, no. 2, pp. 164–168, 2004.

[29] Y. Itoigawa, E. Itoi, Y. Sakoma, N. Yamamoto, H. Sano, and K. Kaneko, "Attachment of the anteroinferior glenohumeral ligament–labrum complex to the glenoid: an anatomic study," *Arthroscopy: The Journal of Arthroscopic & Related Surgery*, vol. 28, no. 11, pp. 1628–1633, 2012.

[30] M. Merila, H. Heliö, L. C. Busch, H. Tomusk, E. Poldoja, A. Eller, K. Kask, T. Haviko, and I. Kolts, "The spiral glenohumeral ligament: an open and arthroscopic anatomy study," *Arthroscopy: The Journal of Arthroscopic & Related Surgery*, vol. 24, no. 11, pp. 1271–1276, 2008.

[31] S. J. O'Brien, M. C. Neves, S. P. Arnoczky, S. R. Rozbruck, E. F. Dicarlo, R. F. Warren, R. Schwartz, and T. L. Wickiewicz, "The anatomy and histology of the inferior glenohumeral ligament complex of the shoulder," *The American journal of sports medicine*, vol. 18, no. 5, pp. 449–456, 1990.

[32] M. N. Simão, M. J. Kobayashi, M. d. A. Hernandes, and M. H. Nogueira-Barbosa, "Evaluation of variations of the glenoid attachment of the inferior glenohumeral ligament by magnetic resonance arthrography," *Radiologia Brasileira*, vol. 54, pp. 148–154, 2021.

[33] A. Koga, Y. Itoigawa, T. Wada, D. Morikawa, K. Ichimura, T. Sakai, T. Kawasaki, Y. Maruyama, and K. Kaneko, "Anatomic analysis of the attachment of the posteroinferior labrum and capsule to the glenoid: A cadaveric study," *Arthroscopy: The Journal of Arthroscopic & Related Surgery*, vol. 36, no. 11, pp. 2814–2819, 2020.

[34] K. L. Moore, A. M. Agur, A. F. Dalley, K. L. Moore *et al.*, "Essential clinical anatomy," p. 433, 2015.

[35] H. Saito, E. Itoi, H. Minagawa, N. Yamamoto, Y. Tuoheti, and N. Seki, "Location of the hill-sachs lesion in shoulders with recurrent anterior dislocation," *Archives of Orthopaedic and Trauma Surgery*, vol. 129, pp. 1327–1334, 2009.

[36] Y.-M. Lho, E. Ha, C.-H. Cho, K.-S. Song, B.-W. Min, K.-C. Bae, K.-J. Lee, I. Hwang, and H.-B. Park, "Inflammatory cytokines are overexpressed in the subacromial bursa of frozen shoulder," *Journal of Shoulder and Elbow Surgery*, vol. 22, no. 5, pp. 666–672, 2013.

[37] T. Bunker and P. Anthony, "The pathology of frozen shoulder. a dupuytren-like disease," *The Journal of Bone & Joint Surgery British Volume*, vol. 77, no. 5, pp. 677–683, 1995.

[38] O. Kilian, U. Pfeil, S. Wenisch, C. Heiss, R. Kraus, and R. Schnettler, "Enhanced alpha1 (i) mrna expression in frozen shoulder and dupuytren tissue," *European journal of medical research*, vol. 12, no. 12, p. 585, 2007.

[39] H. K. Uhthoff and P. Boileau, "Primary frozen shoulder: global capsular stiffness versus localized contracture," *Clinical Orthopaedics and Related Research®*, vol. 456, pp. 79–84, 2007.

[40] Y. Xu, F. Bonar, and G. A. Murrell, "Enhanced expression of neuronal proteins in idiopathic frozen shoulder," *Journal of shoulder and elbow surgery*, vol. 21, no. 10, pp. 1391–1397, 2012.

[41] J.-q. Li, K.-l. Tang, J. Wang, Q.-y. Li, H.-t. Xu, H.-f. Yang, L.-w. Tan, K.-j. Liu, and S.-x. Zhang, "Mri findings for frozen shoulder evaluation: is the thickness of the coracohumeral ligament a valuable diagnostic tool?" *PLoS One*, vol. 6, no. 12, p. e28704, 2011.

[42] J. S. Neviaser, "Arthrography of the shoulder joint: study of the findings in adhesive capsulitis of the shoulder," *jbjs*, vol. 44, no. 7, pp. 1321–1359, 1962.

[43] D. McKean, S. L. Chung, R. te Water Naudé, B. McElroy, J. Baxter, A. Pendse, J. Papanikitas, J. Teh, and R. Hughes, "Elasticity of the coracohumeral ligament in patients with frozen shoulder following rotator interval injection: a case series," *Journal of Ultrasonography*, vol. 20, no. 83, p. e300, 2020.

[44] A. B. Ozbalci and A. Piskin, "Clinical significance of shear wave ultrasound elastography in patients with idiopathic adhesive capsulitis: Can it be used instead of magnetic resonance imaging as an early indicator?" *Ultrasound quarterly*, vol. 38, no. 3, pp. 250–256, 2022.

[45] T. Wada, Y. Itoigawa, K. Yoshida, T. Kawasaki, Y. Maruyama, and K. Kaneko, "Increased stiffness of rotator cuff tendons in frozen shoulder on shear wave elastography," *Journal of Ultrasound in Medicine*, vol. 39, no. 1, pp. 89–97, 2020.

[46] C.-H. Wu, W.-S. Chen, and T.-G. Wang, "Elasticity of the coracohumeral ligament in patients with adhesive capsulitis of the shoulder," *Radiology*, vol. 278, no. 2, pp. 458–464, 2016.

[47] C. Homsi, M. Bordalo-Rodrigues, J. J. Da Silva, and X. M. Stump, "Ultrasound in adhesive capsulitis of the shoulder: is assessment of the coracohumeral ligament a valuable diagnostic tool?" *Skeletal radiology*, vol. 35, pp. 673–678, 2006.

[48] P. Michelin, Y. Delarue, F. Duparc, and J. N. Dacher, "Thickening of the inferior glenohumeral capsule: an ultrasound sign for shoulder capsular contracture," *European radiology*, vol. 23, pp. 2802–2806, 2013.

[49] A. Tandon, S. Dewan, S. Bhatt, A. Jain, and R. Kumari, "Sonography in diagnosis of adhesive capsulitis of the shoulder: a case–control study," *Journal of ultrasound*, vol. 20, pp. 227–236, 2017.

[50] E. Emig, M. E. Schweitzer, D. Karasick, and J. Lubowitz, "Adhesive capsulitis of the shoulder: Mr diagnosis." *AJR. American journal of roentgenology*, vol. 164, no. 6, pp. 1457–1459, 1995.

[51] B. Mengiardi, C. W. Pfirrmann, C. Gerber, J. Hodler, and M. Zanetti, "Frozen shoulder: Mr arthrographic findings," *Radiology*, vol. 233, no. 2, pp. 486–492, 2004.

[52] S. J. Yun, W. Jin, N. S. Cho, K.-N. Ryu, Y. C. Yoon, J. G. Cha, J. S. Park, S. Y. Park, and N. Y. Choi, "Shear-wave and strain ultrasound elastography of the supraspinatus and infraspinatus tendons in patients with idiopathic adhesive capsulitis of the shoulder: a prospective case-control study," *Korean journal of radiology*, vol. 20, no. 7, pp. 1176–1185, 2019.

[53] Y. Yi, K. J. Lee, W. Kim, B.-M. Oh, and S. G. Chung, "Biomechanical properties of the glenohumeral joint capsule in hemiplegic shoulder pain," *Clinical Biomechanics*, vol. 28, no. 8, pp. 873–878, 2013.

[54] J. Zhang, L. Zhang, F. Guo, and T. Zhang, "Shear wave elastography of the coracohumeral ligament with frozen shoulder in different stages," *Journal of Ultrasound in Medicine*, vol. 41, no. 10, pp. 2527–2534, 2022.

[55] V. Ryan, H. Brown, C. J. Minns Lowe, and J. S. Lewis, "The pathophysiology associated with primary (idiopathic) frozen shoulder: A systematic review," *BMC musculoskeletal disorders*, vol. 17, pp. 1–21, 2016.

[56] L. Hollmann, M. Halaki, S. J. Kamper, M. Haber, and K. Ginn, "Does muscle guarding play a role in range of motion loss in patients with frozen shoulder?" *Musculoskeletal Science and Practice*, vol. 37, pp. 64–68, 2018.

[57] T. De Jongh, F. Jongen-Hermus, J. Damen, H. Daelmans, R. Franssen, I. de Klerk-van der Wiel, A. Pieterse, B. J. Schouwenberg, and F. Schuring, *Fysische diagnostiek: uitvoering en betekenis van het lichamelijk onderzoek*. Bohn Stafleu van Loghum, 2015.

[58] B. Erber, N. Hesse, C. Glaser, A. Baur-Melnyk, S. Goller, J. Ricke, and A. Heuck, "Mr imaging detection of adhesive capsulitis of the shoulder: impact of intravenous contrast administration and reader's experience on diagnostic performance," *Skeletal radiology*, vol. 51, no. 9, pp. 1807–1815, 2022.

[59] B. Erber, N. Hesse, S. Goller, F. Gilbert, J. Ricke, C. Glaser, and A. Heuck, "Diagnostic performance and interreader agreement of individual and combined non-enhanced and contrast-enhanced mr imaging parameters in adhesive capsulitis of the shoulder," *Skeletal Radiology*, vol. 53, no. 2, pp. 263–273, 2024.

[60] A. Seth, J. L. Hicks, T. K. Uchida, A. Habib, C. L. Dembia, J. J. Dunne, C. F. Ong, M. S. DeMers, A. Rajagopal, M. Millard *et al.*, "Opensim: Simulating musculoskeletal dynamics and neuromuscular control to study human and animal movement," *PLoS computational biology*, vol. 14, no. 7, p. e1006223, 2018.

[61] A. Seth, M. Dong, R. Matias, and S. Delp, "Muscle contributions to upper-extremity movement and work from a musculoskeletal model of the human shoulder," *Frontiers in neurorobotics*, vol. 13, p. 90, 2019.

[62] A. Dashottar and J. Borstad, "Posterior glenohumeral joint capsule contracture," *Shoulder & elbow*, vol. 4, no. 4, pp. 230–236, 2012.

[63] J. Chen and J. Phadnis, "Glenohumeral capsule and ligaments," *Normal and Pathological Anatomy of the Shoulder*, pp. 93–99, 2015.

[64] D. De la Serna, S. Navarro-Ledesma, F. Alayón, E. López, and L. Pruimboom, "A comprehensive view of frozen shoulder: a mystery syndrome," *Frontiers in medicine*, vol. 8, p. 663703, 2021.

[65] D. Momma, A. Nimura, S. Muro, H. Fujishiro, T. Miyamoto, T. Funakoshi, T. Mochizuki, N. Iwasaki, and K. Akita, "Anatomic analysis of the whole articular capsule of the shoulder joint, with reference to the capsular attachment and thickness," *Journal of Experimental Orthopaedics*, vol. 5, pp. 1–10, 2018.

[66] K. L. Moore, A. M. Agur, A. F. Dalley, K. L. Moore *et al.*, "Essential clinical anatomy," p. 469, 2015.

[67] K. Aliaj, R. L. Lawrence, K. B. Foreman, P. N. Chalmers, and H. B. Henninger, "Kinematic coupling of the glenohumeral and scapulothoracic joints generates humeral axial rotation," *Journal of biomechanics*, vol. 136, p. 111059, 2022.

[68] J. E. Giphart, J. P. Brunkhorst, N. H. Horn, K. B. Shelburne, M. R. Torry, and P. J. Millett, "Effect of plane of arm elevation on glenohumeral kinematics: a normative biplane fluoroscopy study," *JBJS*, vol. 95, no. 3, pp. 238–245, 2013.

[69] P. W. McClure, L. A. Michener, B. J. Sennett, and A. R. Karduna, "Direct 3-dimensional measurement of scapular kinematics during dynamic movements in vivo," *Journal of shoulder and elbow surgery*, vol. 10, no. 3, pp. 269–277, 2001.

[70] M. Fung, S. Kato, P. J. Barrance, J. J. Elias, E. G. McFarland, K. Nobuhara, and E. Y. Chao, "Scapular and clavicular kinematics during humeral elevation: a study with cadavers," *Journal of Shoulder and Elbow Surgery*, vol. 10, no. 3, pp. 278–285, 2001.

[71] M. L. Pearl, S. Jackins, S. B. Lippitt, J. A. Sidles, and F. A. Matsen III, "Humeroscapular positions in a shoulder range-of-motion-examination," *Journal of shoulder and elbow surgery*, vol. 1, no. 6, pp. 296–305, 1992.

[72] A.-T. Hsu, J.-H. Chang, and C.-H. Chang, "Determining the resting position of the glenohumeral joint: a cadaver study," *Journal of Orthopaedic & Sports Physical Therapy*, vol. 32, no. 12, pp. 605–612, 2002.

[73] J. M. Prendergast, S. Balvert, T. Driessen, A. Seth, and L. Peternel, "Biomechanics aware collaborative robot system for delivery of safe physical therapy in shoulder rehabilitation," *IEEE Robotics and Automation Letters*, vol. 6, no. 4, pp. 7177–7184, 2021.

[74] G. R. Huffman, J. E. Tibone, M. H. Mcgarry, B. M. Phipps, Y. S. Lee, and T. Q. Lee, "Path of glenohumeral articulation throughout the rotational range of motion in a thrower's shoulder model," *The American journal of sports medicine*, vol. 34, no. 10, pp. 1662–1669, 2006.

[75] M. H. Metcalf, J. D. Pon, D. T. Harryman II, T. Loutzenheiser, and J. A. Sidles, "Capsulolabral augmentation increases glenohumeral stability in the cadaver shoulder," *Journal of shoulder and elbow surgery*, vol. 10, no. 6, pp. 532–538, 2001.

[76] A. Kewley, J. Beesel, and A. Seth, "Opensim creator (0.5.25) zenodo," 2025.

[77] J. B. Ticker, L. U. Bigliani, L. J. Soslowsky, R. J. Pawluk, E. L. Flatow, and V. C. Mow, "Inferior glenohumeral ligament: geometric and strain-rate dependent properties," *Journal of Shoulder and Elbow Surgery*, vol. 5, no. 4, pp. 269–279, 1996.

[78] R. G. Pollock, V. M. Wang, J. S. Bucchieri, N. P. Cohen, C.-Y. Huang, R. J. Pawluk, E. L. Flatow, L. U. Bigliani, and V. C. Mow, "Effects of repetitive subfailure strains on the mechanical behavior of the inferior glenohumeral ligament," *Journal of shoulder and elbow surgery*, vol. 9, no. 5, pp. 427–435, 2000.

[79] M. Benjamin, H. Toumi, J. R. Ralphs, G. Bydder, T. Best, and S. Milz, "Where tendons and ligaments meet bone: attachment sites ('entheses') in relation to exercise and/or mechanical load," *Journal of anatomy*, vol. 208, no. 4, pp. 471–490, 2006.

6 Appendix A: Wrapping surface radii and examples of issues

CHL and SGHL wrapping surface			
	X	Y	Z
-o	22	22	22
o-	22	22	22
oo	22	22	22
o+	22	22	22
+o	22	22	22

AIGHL wrapping surface			
	X	Y	Z
-o	20	19	20
o-	20	20	19
oo	18	20	21
o+	18	20	21
+o	18	20	21

MGHL wrapping surface			
	X	Y	Z
-o	20	20	20
o-	20	20	20
oo	20	20	20
o+	18	18	18
+o	20	20	20

PIGHL wrapping surface			
	X	Y	Z
-o	18	18	19
o-	18	19	18
oo	20	21	20
o+	20	21	20
+o	19	18	20

Figure 34: These are the X Y and Z radii of the wrapping surfaces that were used in the models

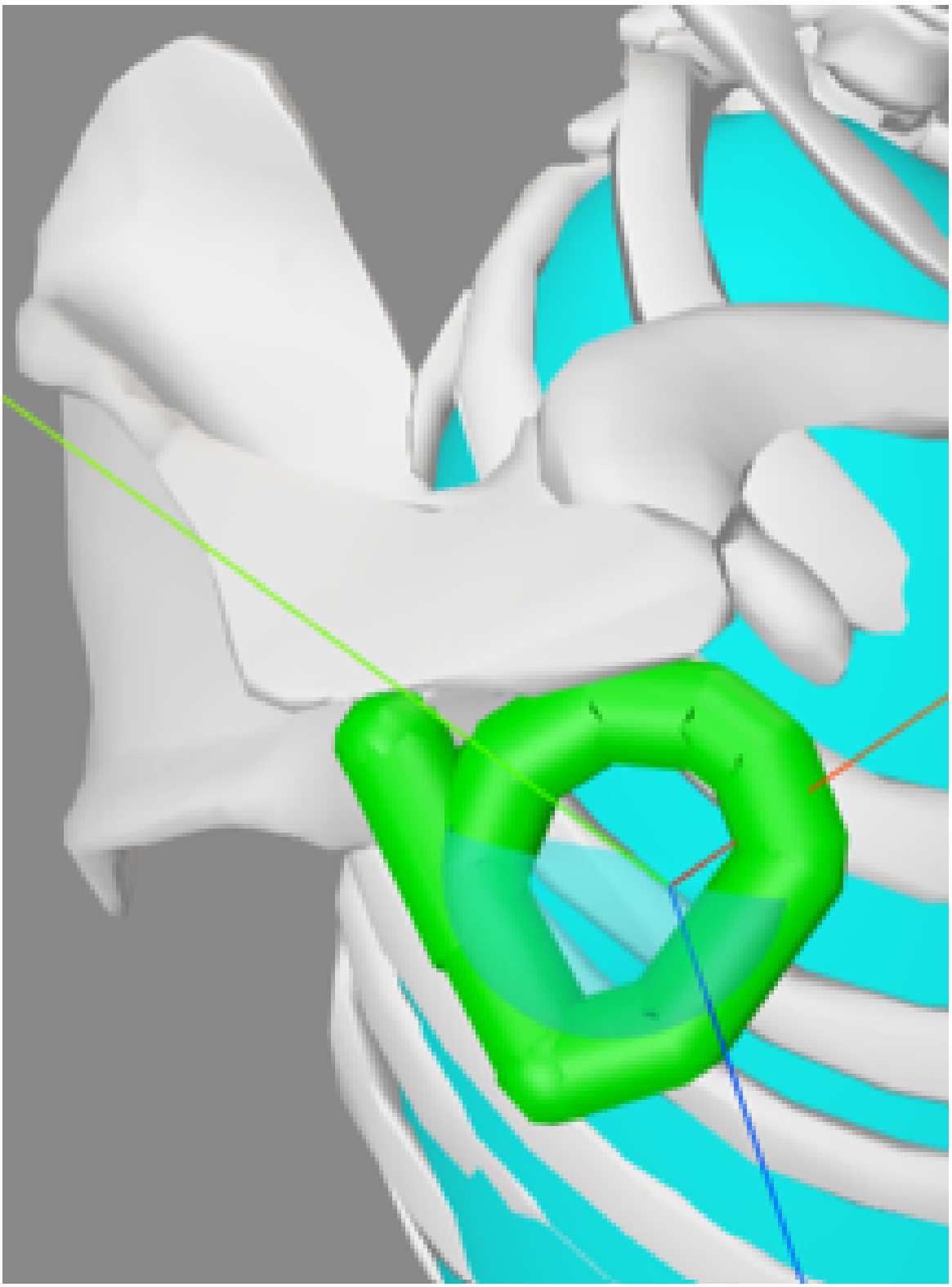

Figure 35: This image is taken from the OpenSim GUI, showing how the wrapping would not be accurate for certain poses

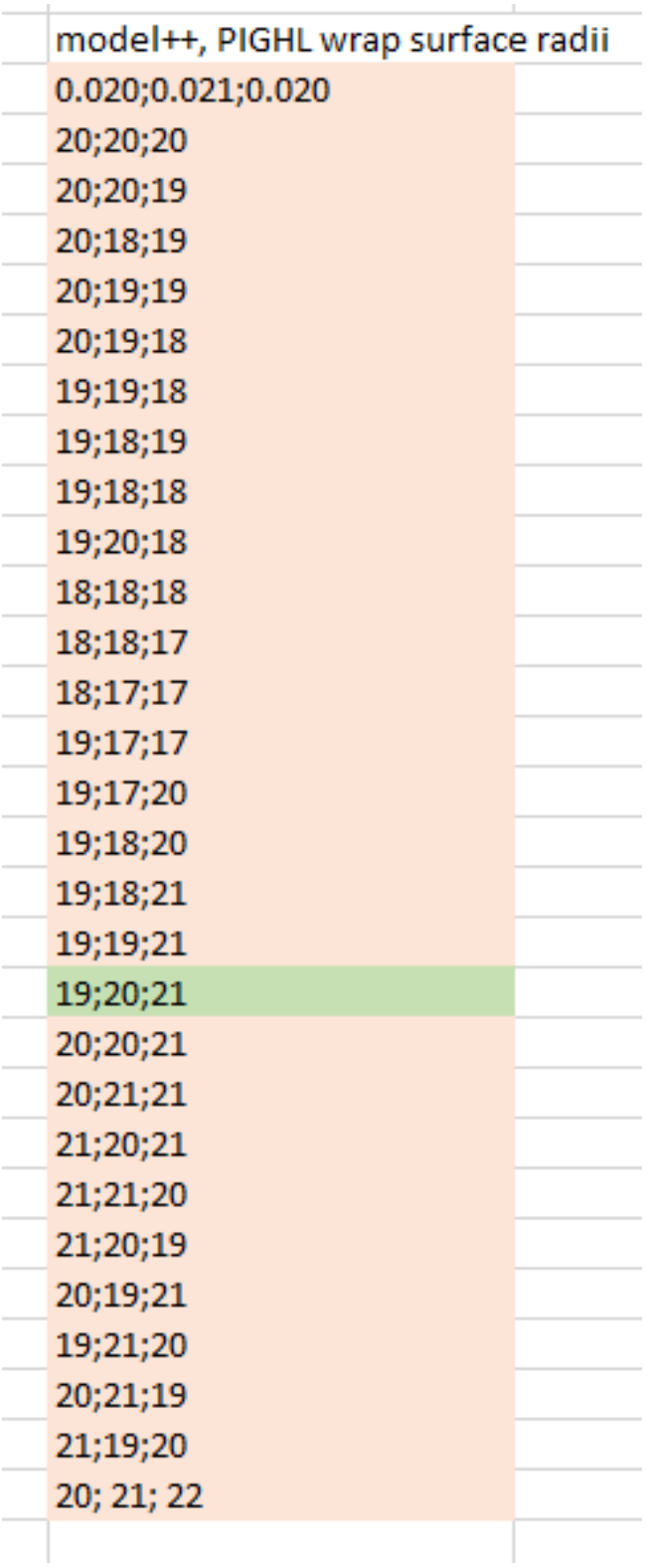

Figure 36: This image shows all the 29 different combinations of wrapping radii that were tried for the PIGHL in the ++ model. Only the green highlighted combination did not result in errors like the one shown in the previous image.